UNITED STATES DEPARTMENT OF THE INTERIOR

GEOLOGICAL SURVEY

Description and Preliminary Testing of the CDSN Seismic Sensor Systems

by

Jon Peterson

and

Edwin E. Tilgner

Open-File Report 85-288

Albuquerque, New Mexico

1985

UNITED STATES DEPARTMENT OF INTERIOR

GEOLOGICAL SURVEY

DESCRIPTION AND PRELIMINARY TESTING OF THE CDSN SEISMIC SENSOR SYSTEMS

Jon Peterson

and

Edwin E. Tilgner

CONTENTS

1. INTRODUCTION

The China Digital Seismograph Network (CDSN) is being designed and installed to provide the People's Republic of China with the facilities needed to create a national digital database for earthquake research. The CDSN, which is being developed jointly by the PRC State Seismological Bureau and the U.S. Geological Survey, will consist initially of nine digitally-recording seismograph stations, a data management system to be used for compiling network-day tapes, and a depot maintenance center. Data produced by the network will be shared with research scientists throughout the world.

A national seismograph network must be designed to support a variety of research objectives. From this standpoint, the choices and tradeoffs involved in specifying signal bandwidth, resolution, and dynamic range are the most important decisions in system design. As in the case of the CDSN, these decisions are made during the selection and design of the seismic sensor system and encoder components. The purpose of this report is to describe the CDSN sensor systems, their important signal characteristics, and the results of preliminary tests that have been performed on the instruments.

Four overlapping data bands will be recorded at each station: short period (SP), broadband (BB), long period (LP), and very long period (VLP). Amplitude response curves are illustrated in Figure 1. Vertical and horizontal components will be recorded for each data band. The SP and LP channels will be recorded with sufficient sensitivities to resolve earth background noise at seismically quiet sites. The BB channels will have a lower sensitivity and are intended for broadband recording of moderate-to-large body-wave signals and for increasing the effective amplitude range in the short- and long-period bands. The VLP channel does not provide additional spectral coverage at long periods; its purpose is to make use of on-site filtration and decimation to reduce post processing requirements for VLP studies. Early plans also included a triaxial set of low-sensitivity accelerometers for recording strong signals from large local and regional earthquakes. The accelerometers are not being installed; however, they may be added in the future.

The short-period signals will be derived from a three-component set of PRC-supplied Model DJ-1 SP seismometers and US-supplied SP amplifiers. The seismometers will be installed in surface or shallow subsurface vaults, except

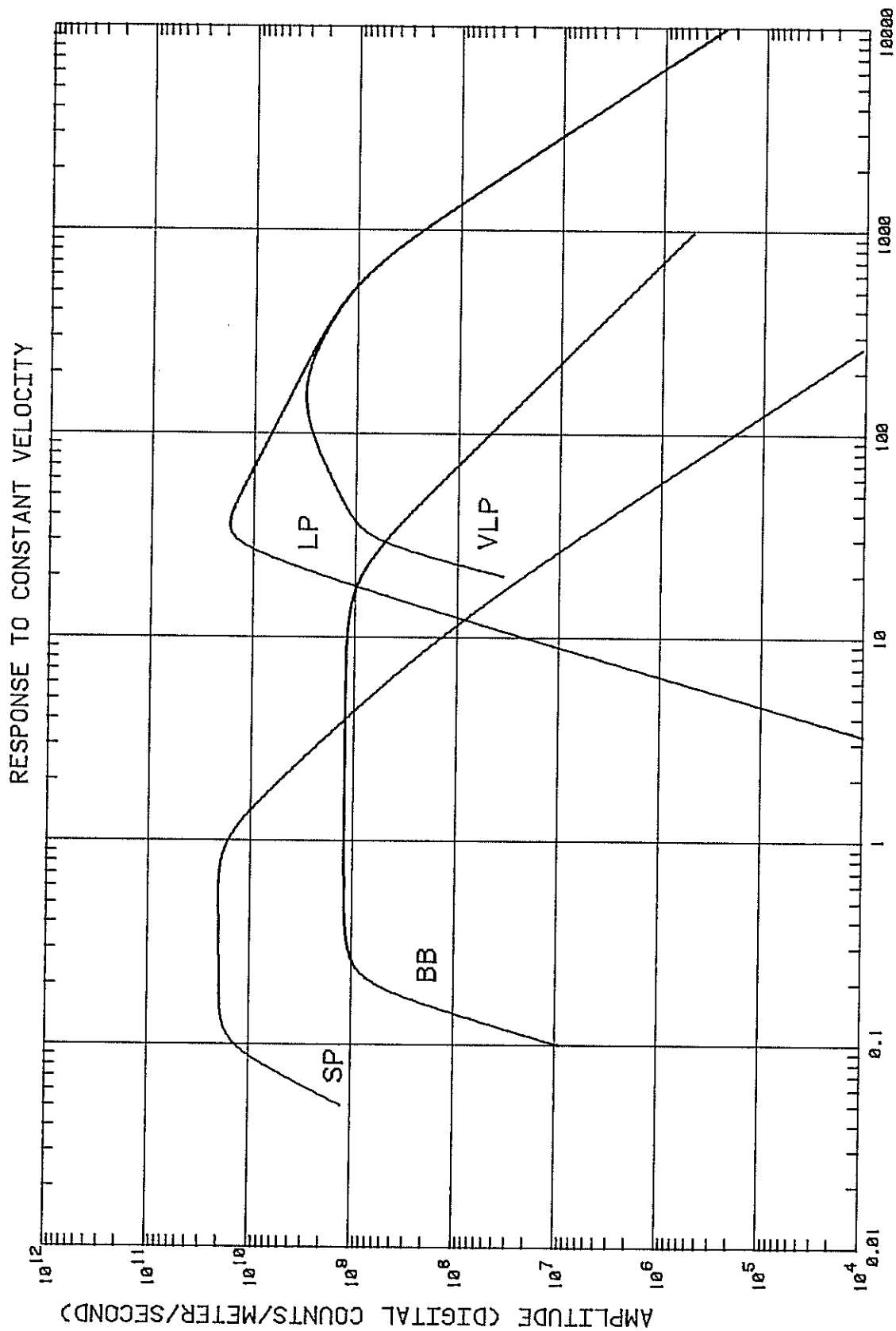

Figure 1.--Amplitude response with respect to earth velocity of data bands to be recorded at the CDSN stations.

at two of the stations where they will be installed in boreholes. The BB, LP, and VLP signals will be derived from Streckeisen STS-1 broadband sensor systems installed in vaults, except at one site where the LP signals only will be derived from a KS-36000 borehole seismometer installed at a depth of 100 meters.

Analog signals will be sampled and quantized by an analog-to-digital converter (ADC) that is part of the recording system. Sampling rates chosen for the CDSN are as follows:

SP	40 samples/second
BB	20 samples/second
LP	1 sample/second
VLP	6 samples/minute

The ADC 16-bit data word format makes use of 14 bits to quantize the signal and 2 bits to specify an automatically ranged gain of 1, 8, 32, or 128. This will provide 84 dB of resolution and up to 42 dB of gain ranging for a total operating range of 126 dB peak to peak.

Magnetic tape cartridges, each having a capacity of 67 megabytes, will be used for recording the digital data. LP and VLP data will be recorded continuously. SP and BB data will be processed through an automatic signal detector of the type described by Murdock and Hutt (1983), and only detected events will be stored on tape. Detection parameters, such as turn-on sensitivity and minimum recording duration for the SP and BB channels, will be fully programmable and easily changed. One or more of the data channels may also be recorded on analog recorders.

A CDSN recording system was not available at the time that the preliminary tests were performed on the CDSN sensor systems. This did not interfere with the principal goals of the testing which were to determine the best sensor installation techniques and to demonstrate the operational performance of the sensor systems, especially with regard to instrument noise and detection capability. When the CDSN recording system is available, additional tests will be performed to measure distortion levels in the full system and components. Distortion tests have been performed on the Streckeisen STS-1 broadband seismometers, the most critical component from the standpoint of linearity, and the results of the tests are reported by Wielandt and Streckeisen (1982). Calibration accuracy and stability are also important sensor system characteristics that cannot be defined without additional testing. These tests will be performed as the instruments are installed at the stations and periodically during operation.

2. SHORT-PERIOD SENSOR SYSTEM

2.1 SP Seismometer

The DJ-1 seismometers (see Figure 2) are recently developed instruments that are manufactured in China. They have pendulum-type suspensions, high-impedance velocity transducers, adjustable period, and their relatively small size makes them suitable for installation in boreholes as well as vaults. The nominal seismometer parameter values are listed in Table 1.

An equivalent circuit for the DJ-1 seismometer is shown in Figure 3 where

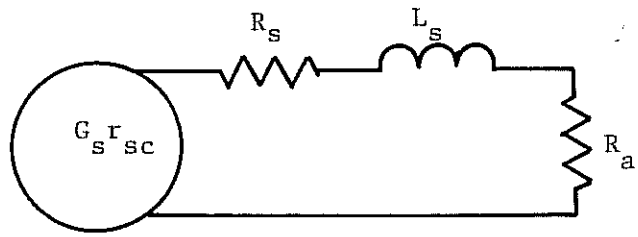

Figure 3.

G_s is the electrodynamic constant of the signal transducer, r_{sc} is the distance from the hinge to the centerline of the signal coil, R_s is the signal coil resistance, L_s is the signal coil inductance, and R_a is the amplifier input resistance, which may be adjusted to set the seismometer damping to a prescribed value. The inductance in the seismometer circuit has the effect of a low-pass filter with a corner frequency at $f_c = (R_s + R_a)/2\pi L_s$ Hz. The coil inductance of the DJ-1 is about 16 henrys and the total circuit resistance is about 290kΩ, so $f_c \approx 3$ kHz. Since this is essentially out of band, the seismometer inductance will not be considered in developing a transfer function for the seismometer.

A block diagram showing signal paths in the seismometer circuit is shown in Figure 4. In the diagram, T(s) represents (in the Laplace domain) an input of torque acting about the seismometer hinge, R_{11} is the total circuit resistance (sum of R_s and R_a), K_s is the moment of inertia of the pendulum about the hinge, λ_{so} is the ratio of air damping to critical damping, ω_s is the natural angular frequency of the seismometer, and $E_s(s)$ represents the seismometer ouput voltage. Then, the transfer function for the seismometer can be expressed as

$$\frac{E_s(s)}{T(s)} = \frac{G_s r_{sc} s}{K_s(s^2 + 2\lambda_{so}\omega_s s + \omega_s^2 + G_s^2 r_{sc}^2 \, s/K_s R_{11})} \quad V/N\cdot m$$

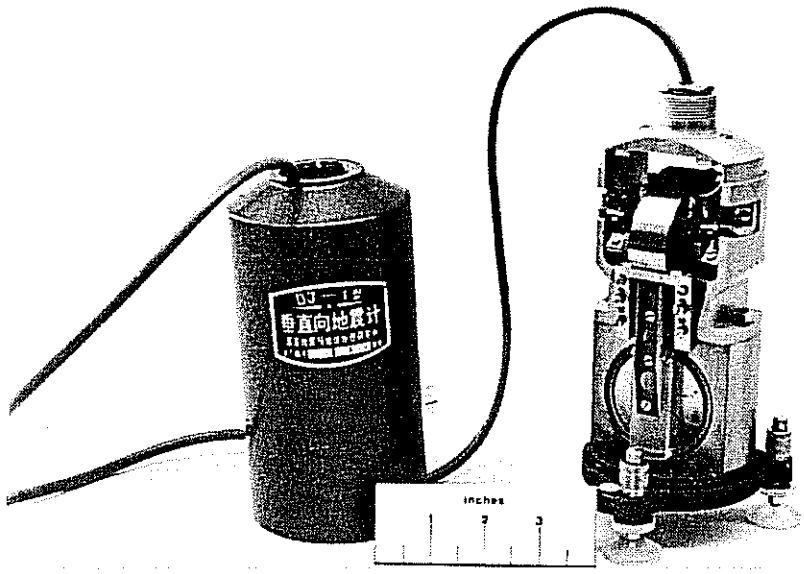

Vertical

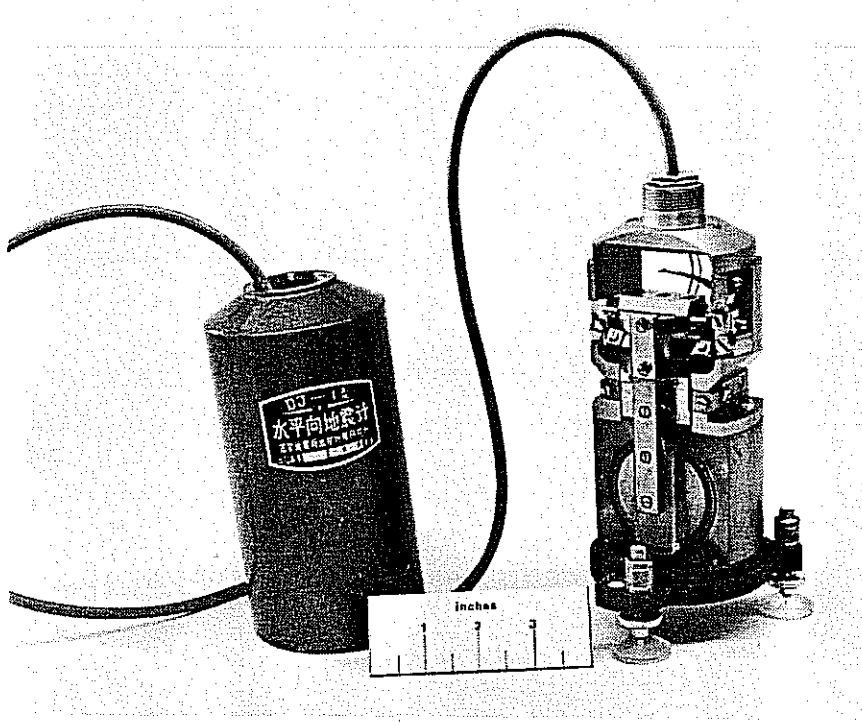

Horizontal

Figure 2.--DJ-1 seismometers.

Parameter	Symbol	Value		Units
		Vertical	Horizontal	
Natural Angular Frequency*	ω_s	6.283	6.283	radians/second
Damping Ratio*	λ_s	0.6	0.6	
Air Damping Ratio	λ_{so}	<.015	<.015	
Inertial Mass	M	.436	.400	kilograms
Hinge to Center of Mass	r_{cm}	.0219	.0160	meters
Moment of Inertia**	K_s	5.45×10^{-4}	3.65×10^{-4}	kilogram-meter^2
Reduced Pendulum Length**	r_{co}	.057	.057	meters
Signal Coil Electrodynamic Constant**	G_s	427	427	volt-seconds/meter
Signal Coil Resistance**	R_s	19,000	19,000	ohms
Hinge to Signal Coil Centerline	r_{sc}	.08	.08	meters
Calibration Coil Electrodynamic Constant**	G_c	1.2	1.2	newtons/ampere
Calibration Coil Resistance	R_c	43	43	ohms
Hinge to Calibration Coil Centerline	r_{cc}	.036	.036	meters

* denotes parameters that must be adjusted during installation.

** denotes that actual values vary from instrument to instrument.

Table 1.--Nominal DJ-1 Seismometer Parameters

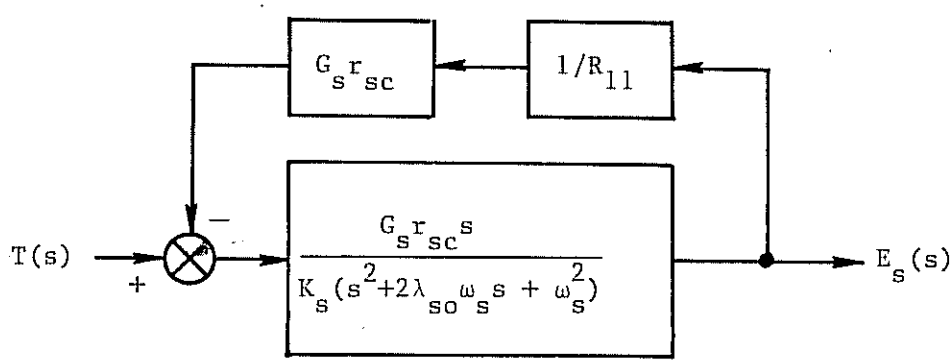

Figure 4.

Letting λ_s represent the ratio of total air and electromagnetic damping to critical damping, the total damping coefficient can be expressed as

$$2\lambda_s\omega_s = 2\lambda_{so}\omega_s + G_s^2 r_{sc}^2/K_s R_{11}$$

so that

$$\frac{E_s(s)}{T(s)} = \frac{G_s r_{sc} s}{K_s(s^2 + 2\lambda_s\omega_s s + \omega_s^2)} \qquad V/N\cdot m$$

During installation, the period of the DJ-1 seismometer is set to 1.0 second. The damping ratio is set to 0.6 by adjusting the amplifier input resistance until the proper overshoot is obtained for a step input. The relationship of overshoot to damping ratio is given by the expression

$$\lambda_s = \delta/(\pi^2 + \delta^2)^{\frac{1}{2}} \quad \text{where } \delta = \ln(e_n/e_{n+1})$$

For a damping ratio of 0.6, the amplitude ratio (e_n/e_{n+1}) of the initial voltage output pulse to its overshoot should be 10.6/1.

For an input of earth velocity, the torque about the hinge can be expressed as

$$T(s) = -Mr_{cm}V_e(s)s \qquad N\cdot m$$

where $V_e(s)$ represents earth velocity, M is the inertial mass of the seismometer, and r_{cm} is the distance from the hinge to the center of mass. Then,

$$\frac{E_s(s)}{V} = \frac{-G_s r_{sc} s^2}{r_{co}(s^2 + 2\lambda_s \omega_s s + \omega_s^2)} \qquad V \cdot s/m$$

where $r_{co} = K_s/r_{cm}$, the distance from the hinge to the center of oscillation (reduced pendulum length).

When a calibration current is applied to the seismometer calibrator, the torque about the hinge is

$$T(s) = G_c r_{cc} I(s) \qquad N \cdot m$$

where I(s) represents the current through the calibrator, G_c is the calibrator motor constant, and r_{cc} is the distance from the hinge to the calibration coil centerline. Then for a calibration input, the transfer function may be expressed as

$$\frac{E_s(s)}{I(s)} = \frac{G_c r_{cc} G_s r_{sc} s}{r_{co}(s^2 + 2\lambda_s \omega_s s + \omega_s^2)} \qquad V/A$$

A calibration current is equivalent to an input of earth motion, and the relationship is established by letting the torques be equal as follows

$$-Mr_{cm} V_e(s) = G_c r_{cc} I(s)$$

For a steady-state sine-wave calibration, the earth motion equivalent to the calibration current, i_c, is

$$A_c = V_c \omega = D_c \omega^2 = G_c r_{cc} i_c / M r_{cm} \qquad m/s^2$$

where A_c, V_c, and D_c are equivalent acceleration, velocity, and displacement for a calibration current applied at an angular frequency of ω radians/second. A steady-state sine-wave calibration will be used during installation to adjust the sensitivities of the short-period sensor systems to prescribed common values that will depend on earth background noise levels at each site.

2.2 SP Amplifier

Short-period signals are amplified and filtered in Teledyne Geotech Model 56130 SP amplifiers. These are low-noise amplifiers with the high input impedance needed to match the DJ-1 seismometers. The three amplifiers that will be used at each station are mounted together with a regulated power supply and connector panel in a shielded and sealed enclosure that will be installed in the vault near the seismometers.

The Model 56130 amplifier specifications are given in Table 2. Each amplifier has two outputs, one for the ADC and one for an analog recorder. The ADC output has a gain of 60 dB (single ended). This can be attenuated in 6 dB steps over a range of 36 dB, and there is a 12 dB trim attenuator that will be used to equalize the recording sensitivities of all channels. The analog output has the same frequency response as the ADC output, but with an additional 18 dB of gain.

Response shaping in the amplifier is provided by a single-pole high-pass filter cornered at 0.1 Hz to eliminate offset and a 4-pole Butterworth low-pass filter cornered at 10 Hz that provides 24 dB of attenuation at the Nyquist frequency. If $E_o(s)$ represents the voltage out of the amplifier and G_{spa} is the amplifier gain

$$\frac{E_o(s)}{E_s(s)} = G_{spa} \cdot \frac{1.559 \times 10^7}{(s^2 + 116.1s + 3948)(s^2 + 48.1s + 3948)} \cdot \frac{s}{(s + .6283)} \quad V/V$$

Amplitude and phase responses, computed from the transfer function, are illustrated in Figure 5. The points on the amplitude curve represent average values of measured data taken from five of the amplifiers.

2.3 SP Transfer Function

The transfer function for the short-period sensor system is the product of the seismometer and amplifier transfer functions and the digital encoder sensitivity, K_{adc}. For the CDSN recording system, $K_{adc} = 1 \times 10^5$ digital counts (DC) per volt. Letting SPTF(s) represent the SP transfer function (encoder output as a function of earth velocity),

$$SPTF(s) = K_{adc} \cdot \frac{E_s(s)}{V_e(s)} \cdot \frac{E_o(s)}{E_s(s)} \quad DC \cdot s/m$$

Input:	Balanced
Input Impedance:	Greater than 10^{12} ohms, adjustable to any desired value from 0 to 10^{7} ohms by soldering in a fixed resistor across the input on terminal posts.
Common Mode Rejection:	100 dB minimum
Dynamic Range:	120 dB minimum
Linearity:	.01% or less
Gain:	24 to 60 dB in 7 steps, 6 dB per step, with an additional 12 dB of trim range.
Output:	Balanced or single ended
Output Balance:	Adjustable
Output Level:	$\pm$ 10 volts with 2,000 ohm load, balanced
Output Impedance:	10 ohms, short-circuit protected.
Output Noise Level:	30 microvolts per $Hz^{\frac{1}{2}}$ at 1 Hz maximum with input shorted and gain set to maximum (60 dB). 60 microvolts per $Hz^{\frac{1}{2}}$ maximum at 1 Hz with input terminated with 60 Kohms, maximum gain.
Response:	Four-pole low-pass Butterworth filter with corner frequency at 10 Hz; one-pole high-pass filter with corner frequency at 0.1 Hz.

Table 2.--Short-period amplifier specifications.

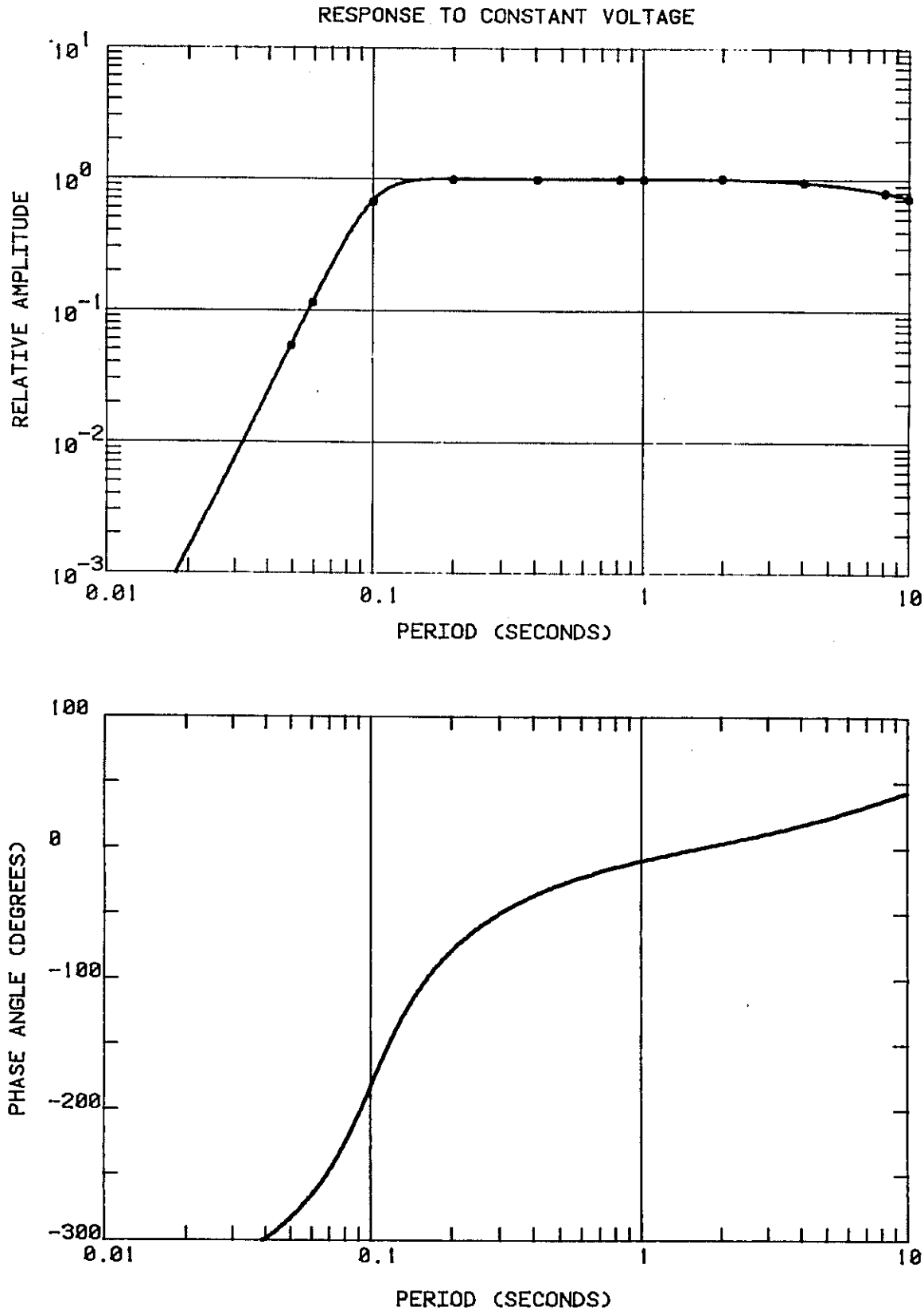

Figure 5.--Amplitude and phase responses computed for the Teledyne-Geotech Model 56130 SP amplifiers. Points on the amplitude curve are average measured values.

or,

$$SPTF(s) = \frac{G_s r_{sc}}{r_{co}} \cdot G_{spa} \cdot K_{adc} \cdot \frac{s^2}{s^2 + 7.54s + 39.48}$$

$$\cdot \frac{1.559 \times 10^7}{(s^2 + 116.1s + 3948)(s^2 + 48.1s + 3948)} \cdot \frac{s}{s + .6283} \quad DC \cdot s/m$$

The poles and zeros of the SP transfer function are listed in Table 3. The relative amplitude response and phase response, computed from the transfer function using nominal instrument parameters, are illustrated in Figure 6. The points on the amplitude response curve are average measured values taken from four test systems.

At quiet sites, the digital velocity sensitivity will be set by letting

$$\frac{G_s r_{sc}}{r_{co}} \cdot G_{spa} \cdot K_{adc} = 2 \times 10^{10} \quad DC \cdot s/m$$

At a period of one second the displacement sensitivity will be 1×10^{11} DC/m. This is likely to be the highest recording sensitivity used in the network. At sites with higher background noise levels, the operating sensitivity will be lowered in order to optimize the operating range (background to clipping).

The standard sensitivity is set by adjusting the amplifier attenuation. For a digital sensitivity of 2×10^{10} DC·s/m, the voltage sensitivity at the output of the amplifier will be 2×10^5 V·s/m. When the amplifier attenuator is properly adjusted, a 5-Hz calibration input current equivalent to 5×10^{-6} m/s (V_c) will produce a 1-volt output. The appropriate peak-to-peak calibration current is found from the relation

$$i_c = \frac{V_c M r_{cm} \omega}{G_c r_{cc}} \quad A$$

and it will vary from instrument to instrument. For nominal instrument parameters (vertical component), the proper calibration current will be 3.47×10^{-5} amperes and the gain of the amplifier will have to be adjusted to 333.3 (50.5 dB). The amplifier trim attenuator is used to compensate for differences in seismometer constants.

During installation of the SP sensor systems and periodically thereafter,

Poles	Zeros
-3.770 + j(5.026)	0.000 + j(0.000)
-3.770 - j(5.026)	0.000 + j(0.000)
-58.05 + j(24.05)	
-58.05 - j(24.05)	
-24.05 + j(58.05)	
-24.05 - j(58.05)	
-.6283 + j(0.000)	0.000 + j(0.000)

Table 3.--Short-period transfer function poles and zeros for an input of earth velocity.

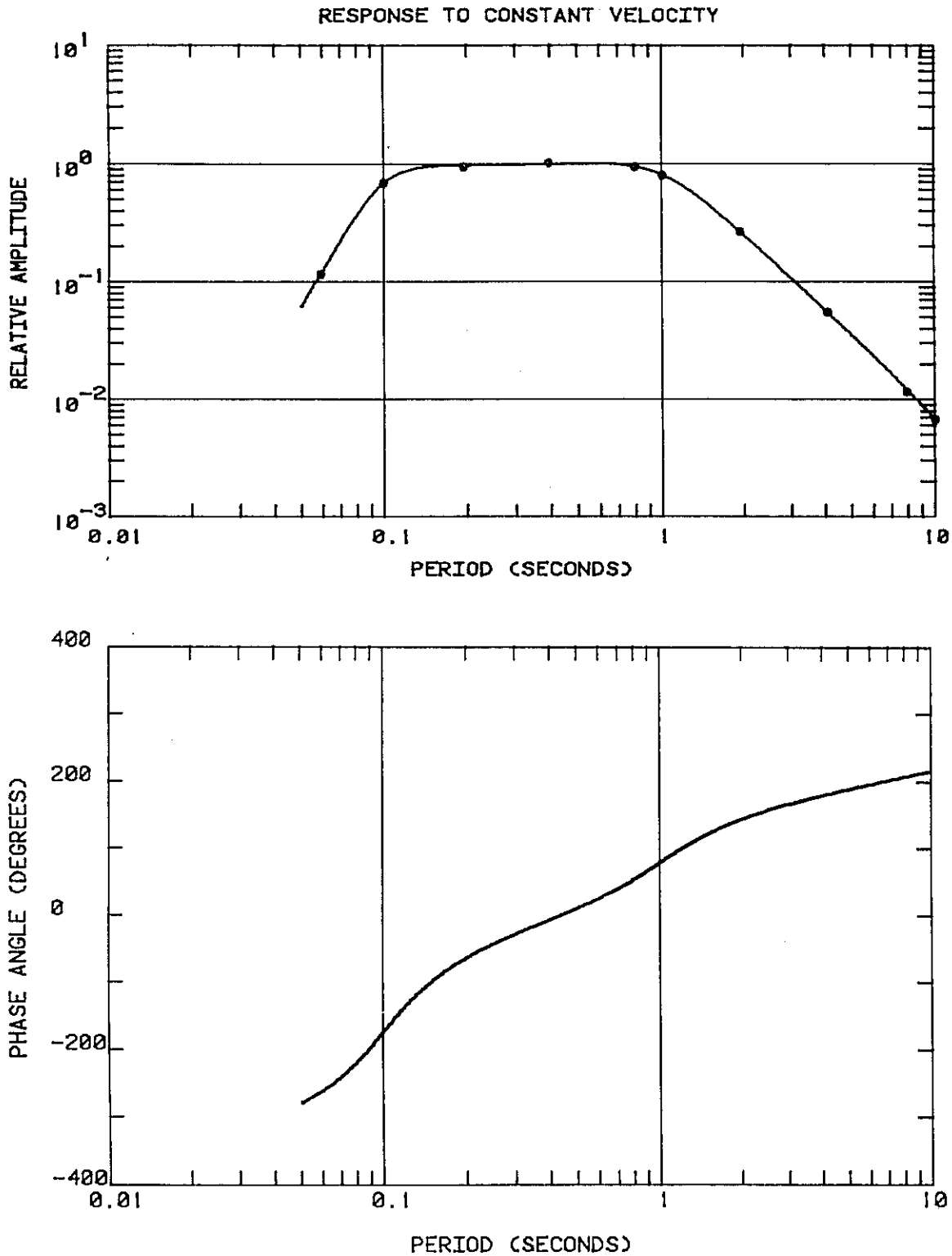

Figure 6.--Amplitude and phase responses of the SP sensor system computed from the transfer function. Points on the amplitude curve are average measured values.

the transfer function will be verified using steady-state sinusoidal calibration inputs at several frequencies. A step function input will be used for routine calibration. For the first several months of operation, step function inputs will be applied daily. When the stability of the step response is demonstrated, indicating negligible instrument parameter drift, the frequency of the step calibration will be reduced. The amplitude of the step input will be adjusted such that the peak step response is about one half of full scale, insuring a good signal-to-noise ratio. Examples of computed and measured step responses are shown in Figure 7. Analysis of the step response can be automated. The stability of parameters most likely to drift (seismometer period and sensitivity constants) can be monitored by measurement of the peak amplitude of the step response, and with a good signal-to-noise ratio it should be possible to derive individual transfer functions from the step responses through direct Fourier transformation or by least-squares fitting.

2.4 SP System Operational Tests

2.4.1 Introduction

The purpose of operational testing is to verify that system components meet their design specifications and that they function together to produce data of acceptable quality. One of the desirable attributes of a sensitive short-period sensor system is the resolution of signals at earth background levels throughout the short-period band, in this case from 0.1 Hz to the Nyquist frequency (20 Hz). An evaluation of system noise and detection capability has been a major part of the testing activity.

Operational tests were performed on four DJ-1 seismometers (two vertical and two horizontal) provided by the State Seismological Bureau and the short-period amplifiers manufactured by Teledyne Geotech for the CDSN project. During the tests, a Teledyne Geotech S-13 short-period seismometer was operated in parallel with the DJ-1 seismometers to provide an independent set of data. Analog signals were digitized and recorded on a Kinemetrics PDR-2 digital event recorder. The seismometers, amplifiers, and the PDR-2 recorder were installed together in a subsurface vault at the Albuquerque Seismological Laboratory.

2.4.2 Amplifier Noise

Noise power was measured at the outputs of five short-period amplifiers and found to be approximately the same level in all cases. A typical example is shown in Figure 6. During the tests, the amplifiers and seismometers were

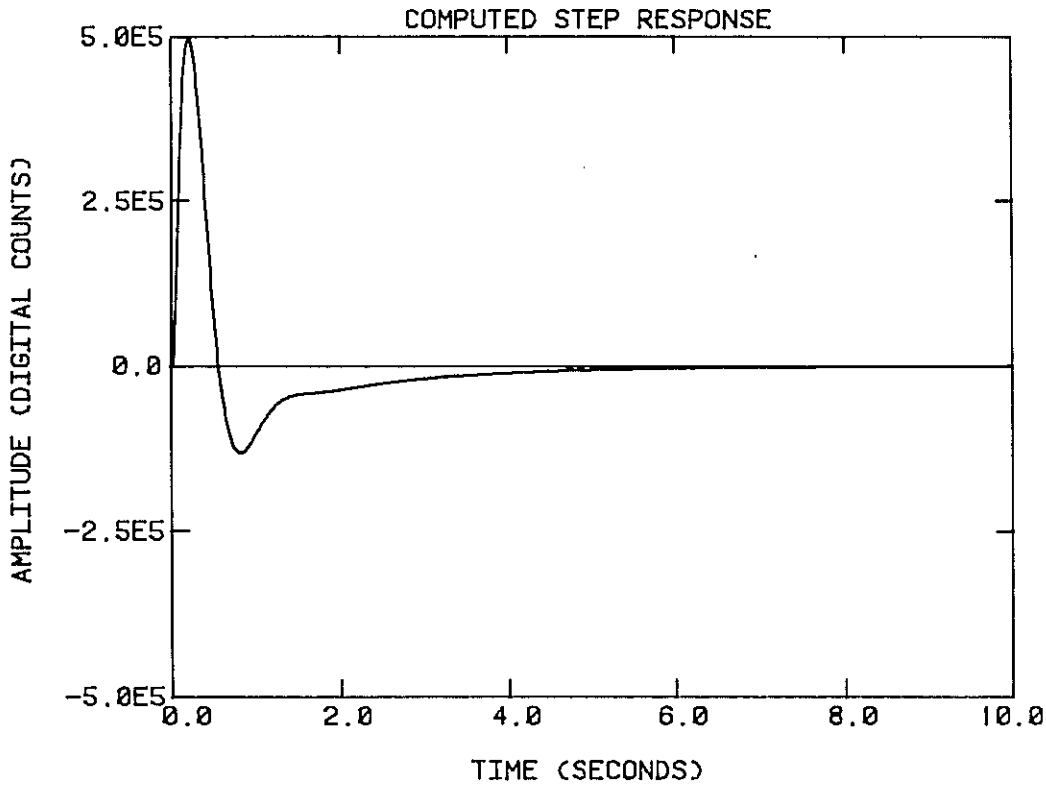

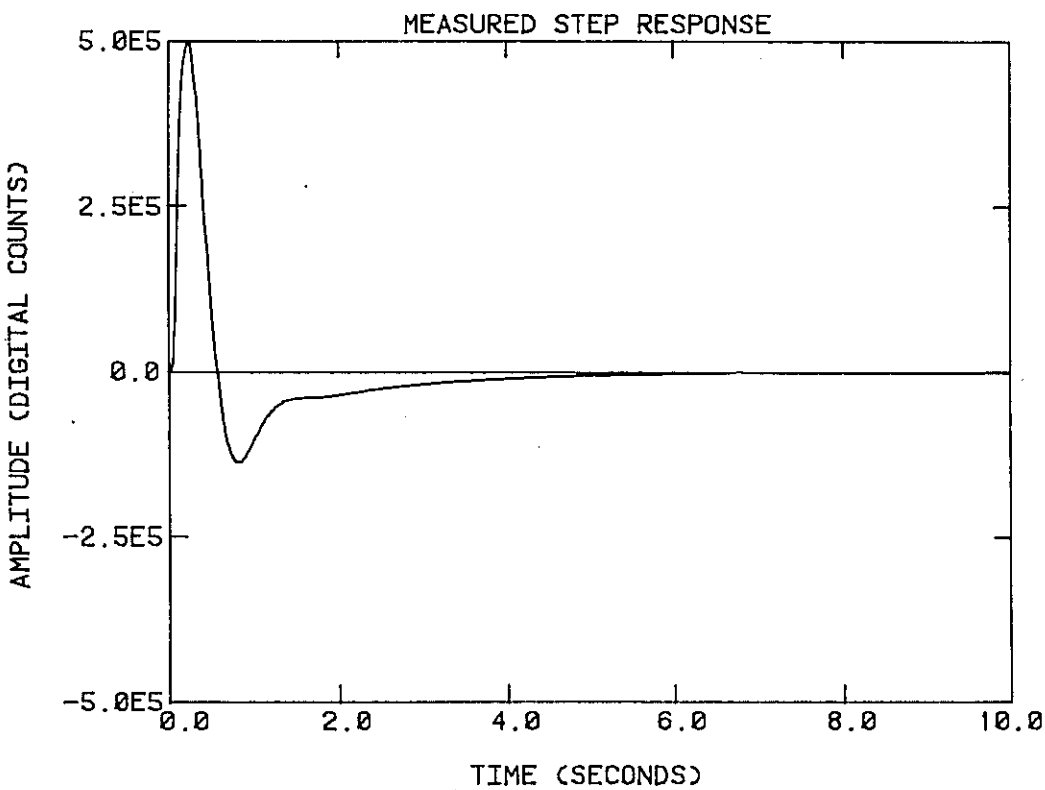

Figure 7.--Examples of computed and measured step responses with amplitudes normalized to one half of full scale. The computed step response is derived by convolving a step function with the system impulse response.

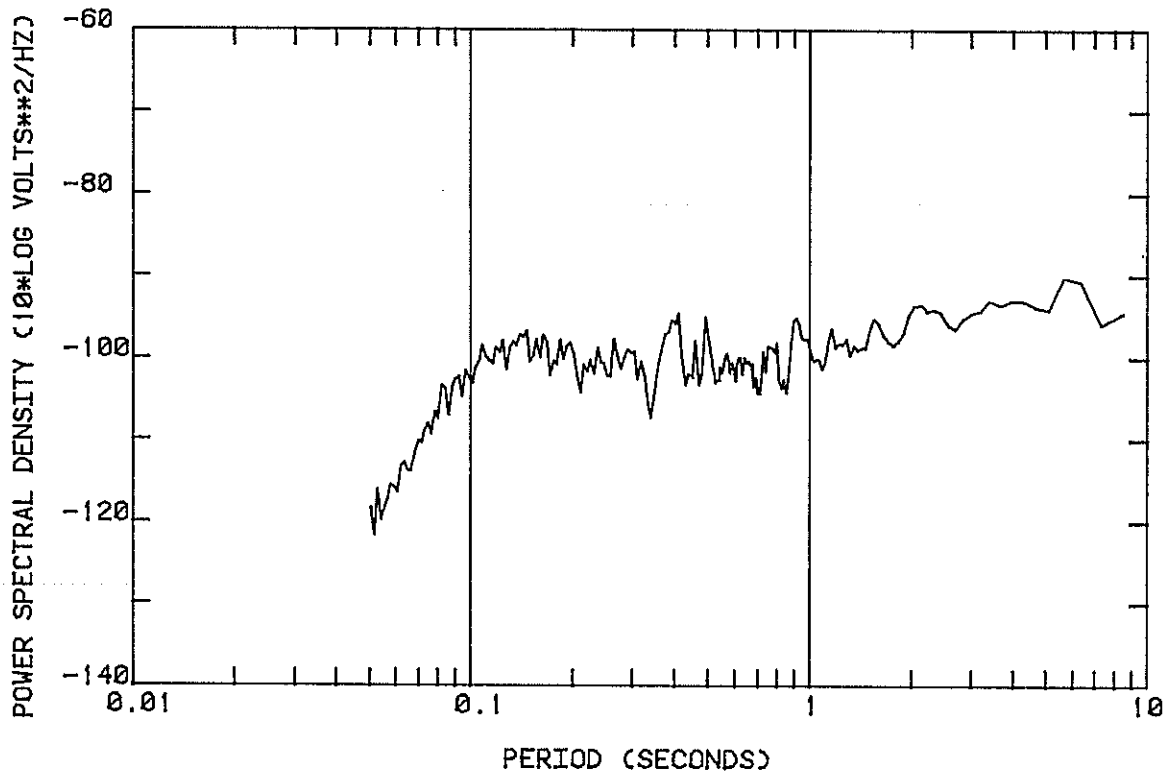

Figure 8.--Typical noise power measured at the output of the short-period amplifier with the seismometer mass blocked. Amplifier gain is 50 dB.

connected as in normal operation, but the seismometer masses were blocked. Amplifier gain was adjusted to 50 dB, the highest gain that will be used in the network. Although this procedure is somewhat different than the procedure described in the amplifier specifications (Table 2), the output of approximately 30 microvolts per root Hz at 1 Hz is within the acceptable range of noise power prescribed in the specifications.

A more useful illustration of amplifier noise is shown in Figure 9. The curve labeled AMP in the figure is based on the spectral data shown in Figure 8, but corrected for instrument response so that the spectral estimate is shown in equivalent units of earth displacement power. The curve labeled PDR-2 in Figure 9 is the least-count noise measured by shorting the input to the digital recorder. It also has been corrected for instrument response. The reference curve labeled LNM (low-noise model) will be used throughout this report to represent earth background noise at a quiet site. The LNM curve is a straight-line approximation of noise spectra published by Li and others (1984) for the period range from .04 to 0.4 seconds, by Peterson (1980) for the period range from 0.4 to 100 seconds, and by Agnew and Berger (1978) for periods greater than 100 seconds. Based on the LNM curve, as shown in Figure 9, earth noise could be masked by amplifier noise at periods below 0.1 second. However, there are few known sites where earth background noise tracks the LNM curve in this period range.

2.4.3 System Noise

The four DJ-1 seismometers were installed in the vault with the two horizontal seismometers in parallel. Seismometer period and damping were adjusted to prescribed values and amplifier gains were set to approximately 50 dB, depending on the sensitivity of the seismometer. Segments of data were recorded on the PDR-2 during nighttime hours when the background noise level is lowest and during daytime hours when the background is higher because of increased cultural activity.

Typical waveforms from the DJ-1 vertical-component seismometers recorded during a nighttime period are shown in Figure 10. The displacement power spectral densities, derived by averaging spectral estimates computed from ten 2048-point overlapping data segments, are plotted together in Figure 11, and the coherence function is plotted in Figure 12. The signal-to-noise ratio in the period range from .05 to 0.1 seconds is about 12 dB (assuming equal noise power in the test systems), which is more than adequate for resolving signals at locations having background noise levels similar to those at the Albuquerque observatory.

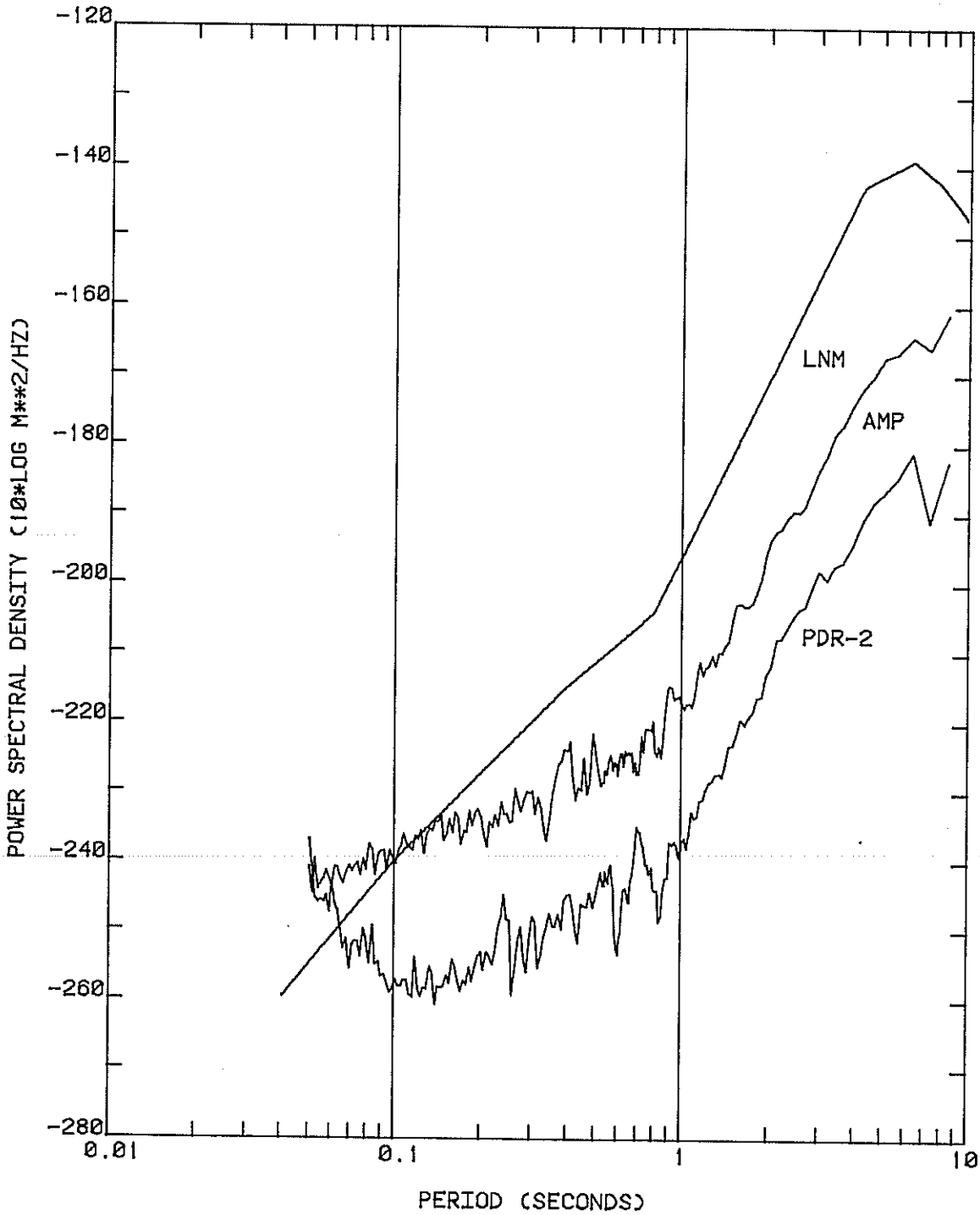

Figure 9.--Typical amplifier noise (AMP) and least-count noise (PDR-2) expressed in equivalent units of displacement power spectral density and compared with a low earth noise model (LNM).

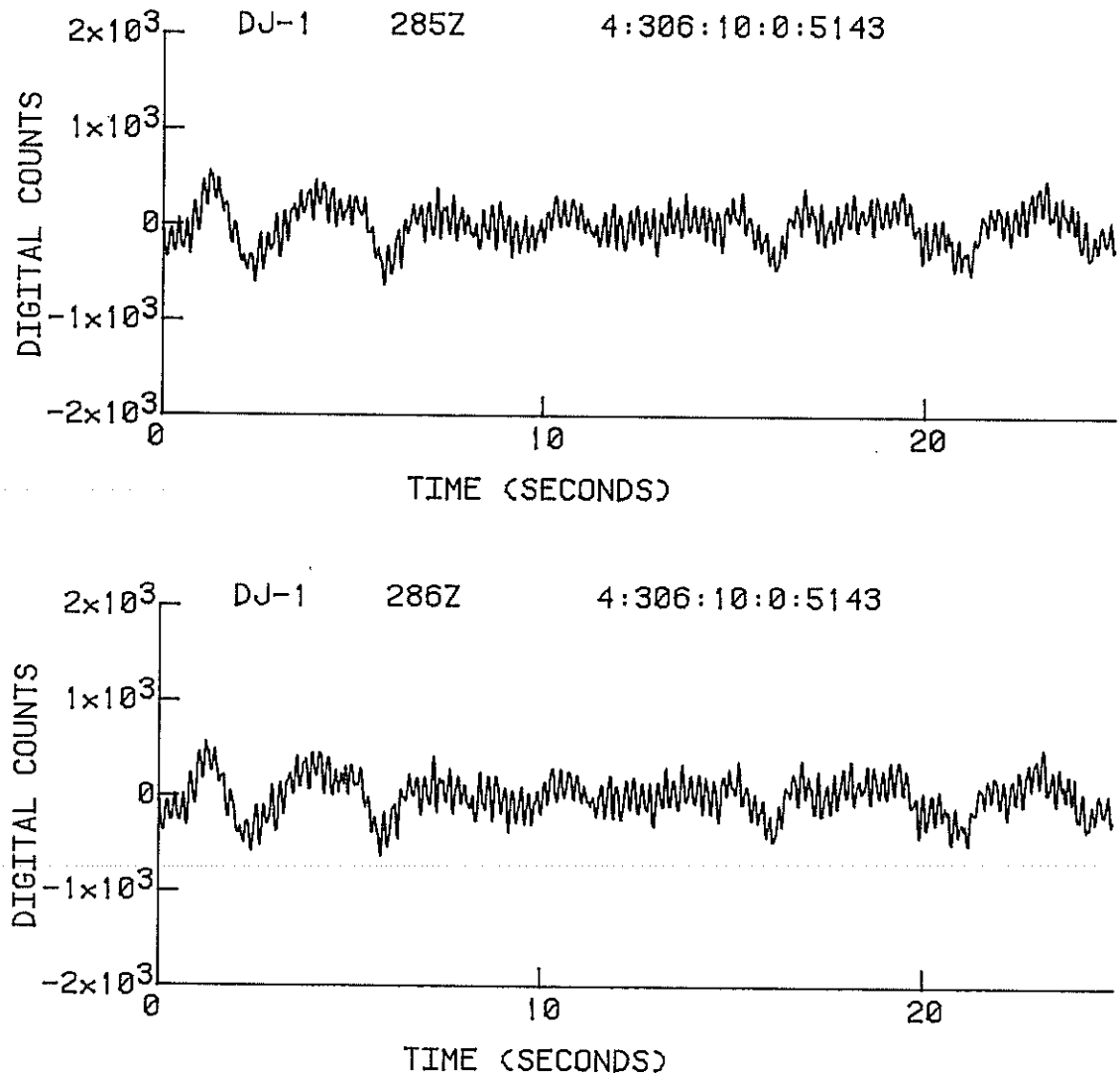

Figure 10.--Sample signal waveforms taken from two vertical-component DJ-1 seismometers operated side by side during a quiet nighttime period. Magnification of the trace at a period of 2.5 seconds (period of the dominant microseism) is about 250K, and magnification of the trace at 0.2 seconds (period of the dominant cultural noise) is about 14M.

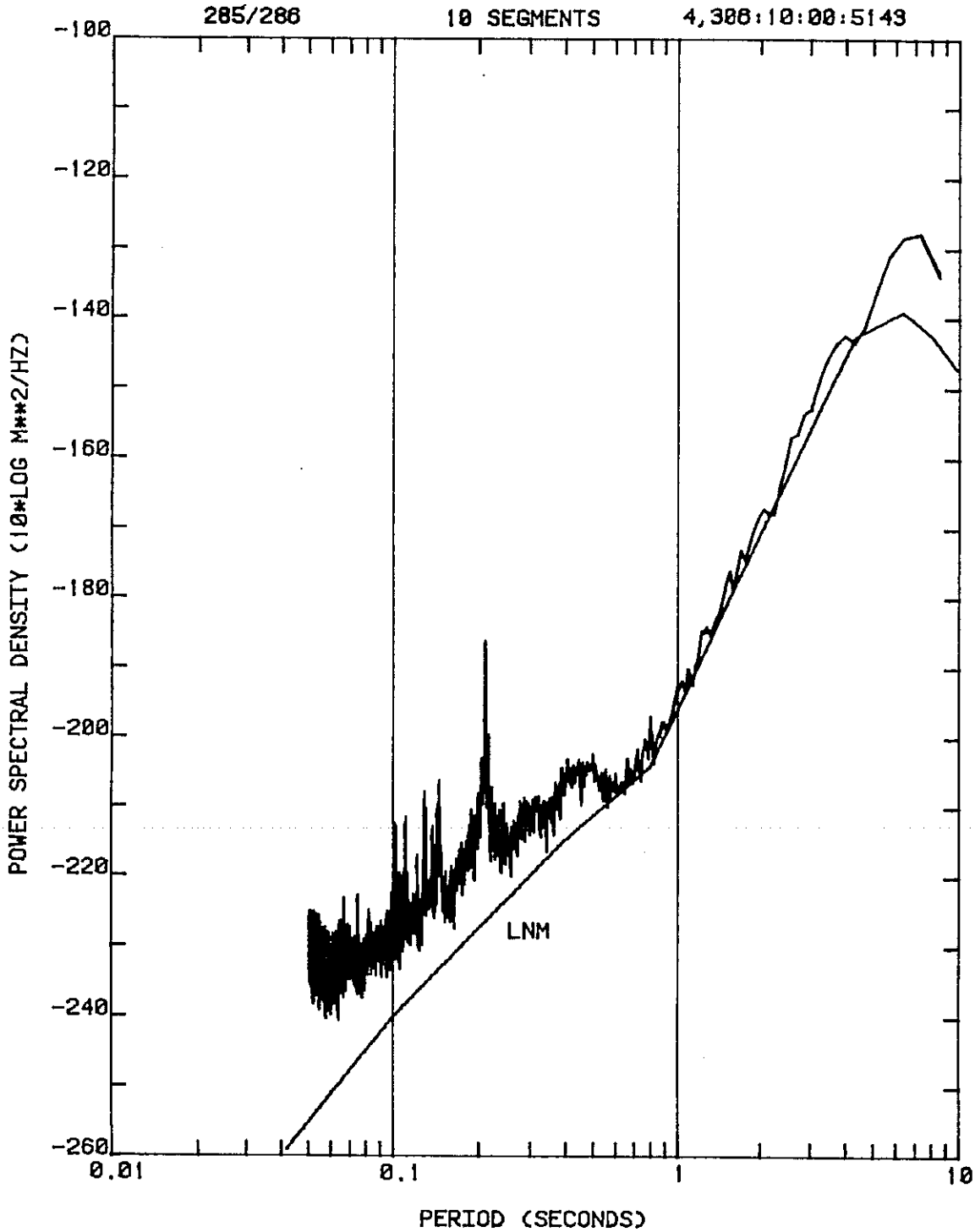

Figure 11.--Power spectral densities computed from signals taken from two vertical DJ-1 seismometers during a quiet period. The LNM curve is shown for comparison.

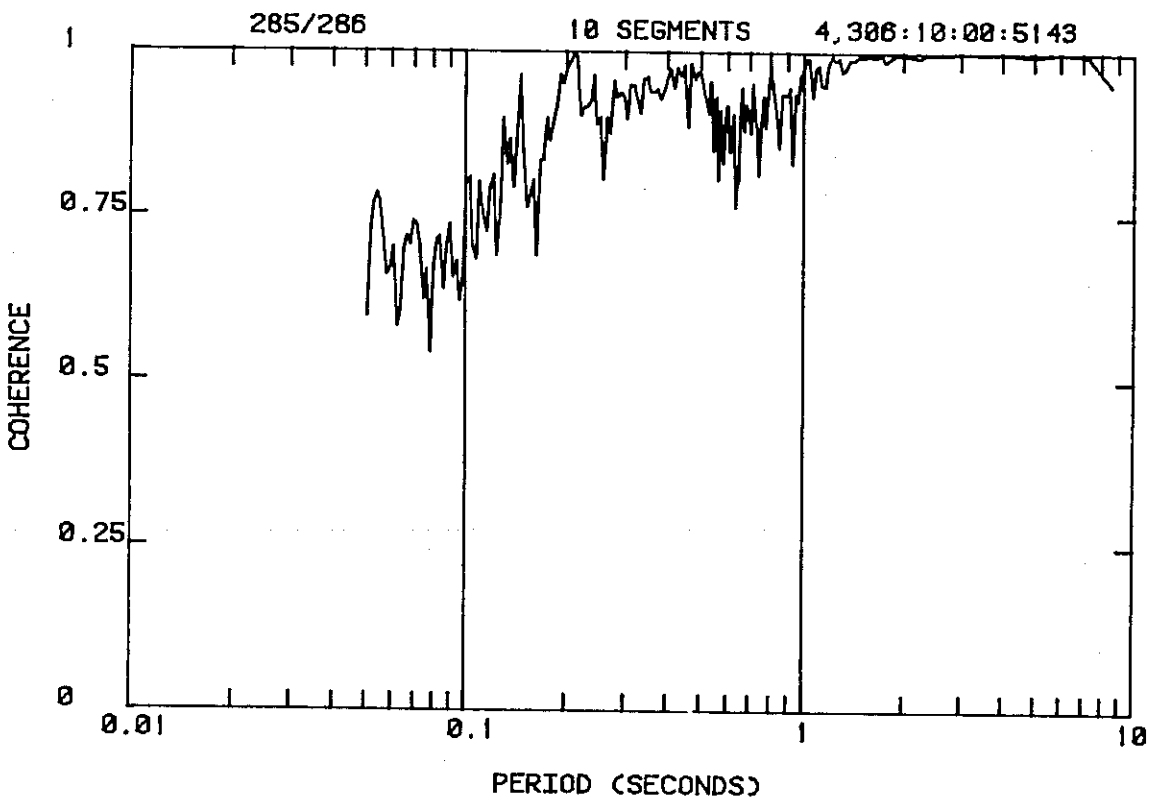

Figure 12.--Coherence between signals taken from two DJ-1 vertical seismometers during a quiet period.

Sample waveforms, displacement power spectral densities, and the coherence of signals taken from the vertical-component test systems during noisier daytime hours are shown in Figures 13 through 15. As expected, the increased background noise at periods less than one second results in an increase in coherence between signals taken from the parallel test systems.

Sample waveforms, displacement power spectral densities, and the coherence of signals taken from the horizontal-component test systems during a quiet nighttime period are shown in Figures 16 through 18. There are no important differences between the horizontal and vertical DJ-1 components with respect to noise levels and detection capability. Although not shown, the coherence between horizontal-component signals during noisier daytime hours also increases.

As stated earlier, an S-13 seismometer was operated in parallel with the DJ-1 seismometers during the tests. There were no observable differences between signals from the S-13 and DJ-1 seismometers.

Based on the test results, our conclusion is that the combination of the DJ-1 seismometer and the Model 56130 amplifier is a suitable short-period sensor system for the CDSN. However, installation methods used at the stations could affect data quality. The high impedance seismometer-amplifier coupling circuit makes the sensor system susceptible to induced electrical noise, especially if the cables are long and not properly shielded and grounded.

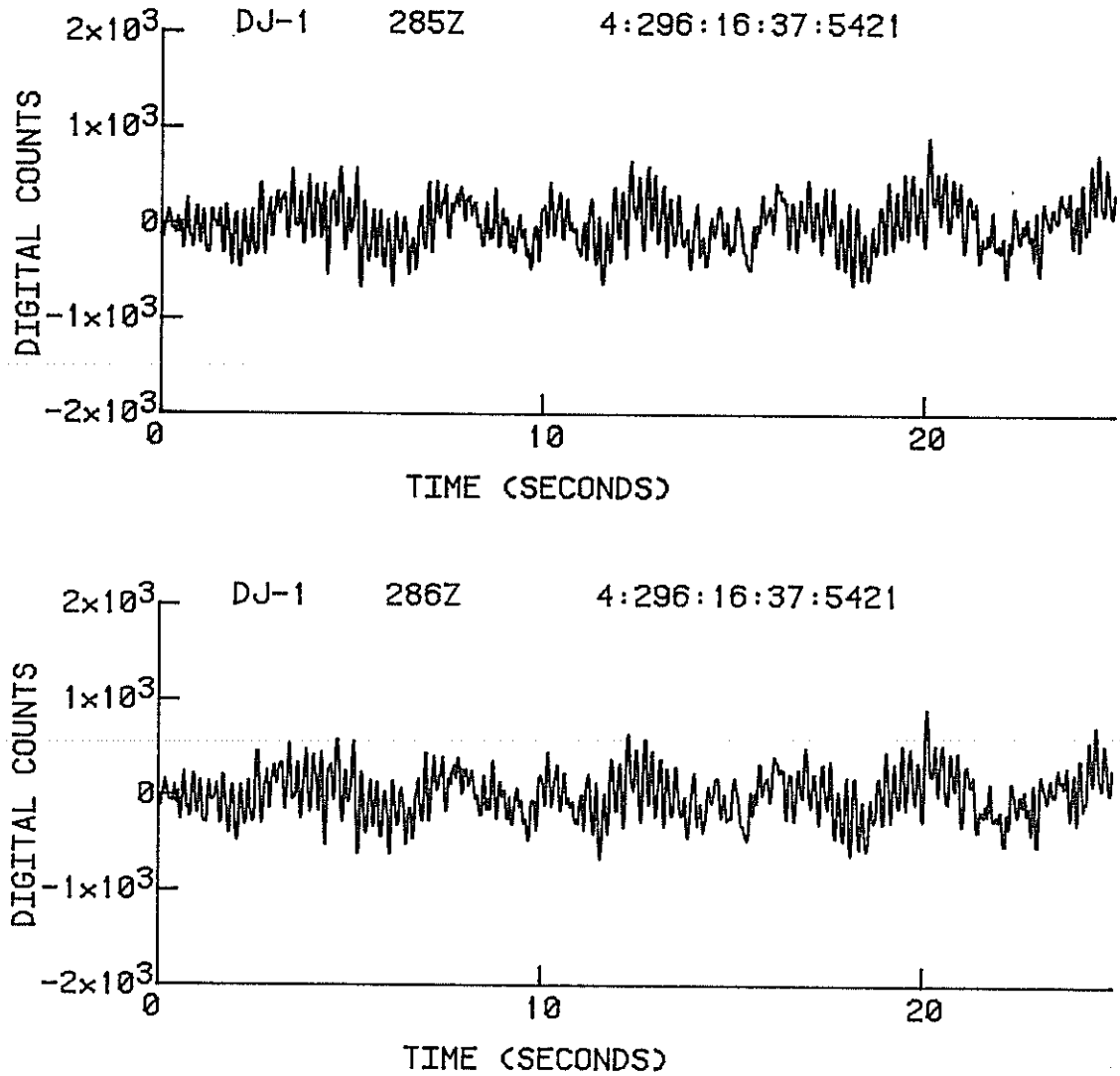

Figure 13.--Sample signal waveforms taken from two vertical-component DJ-1 seismometers operated side by side during daytime hours.

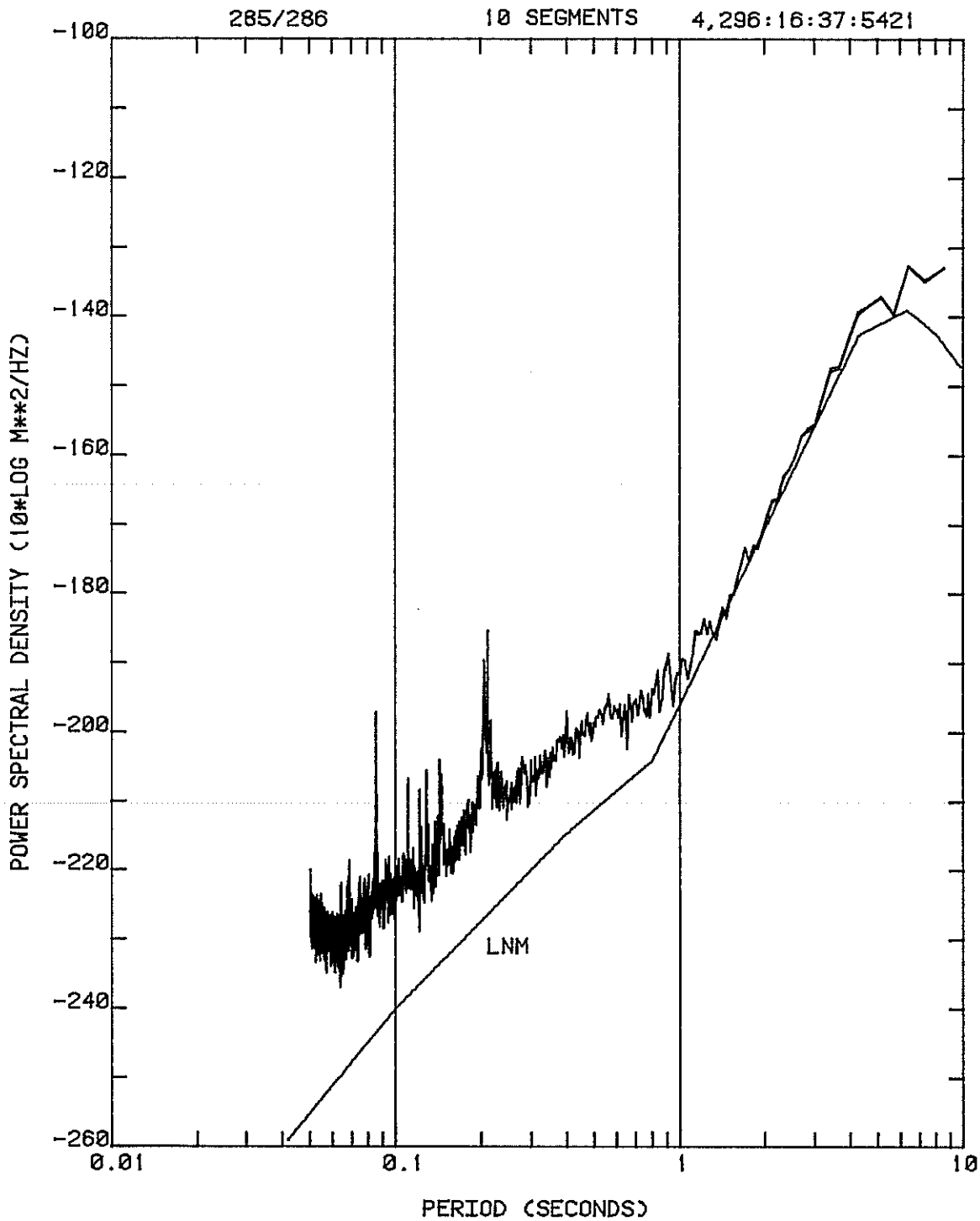

Figure 14.--Power spectral desnities computed from signals taken from two vertical DJ-1 seismometer during a daytime period. The LNM curve is shown for comparison.

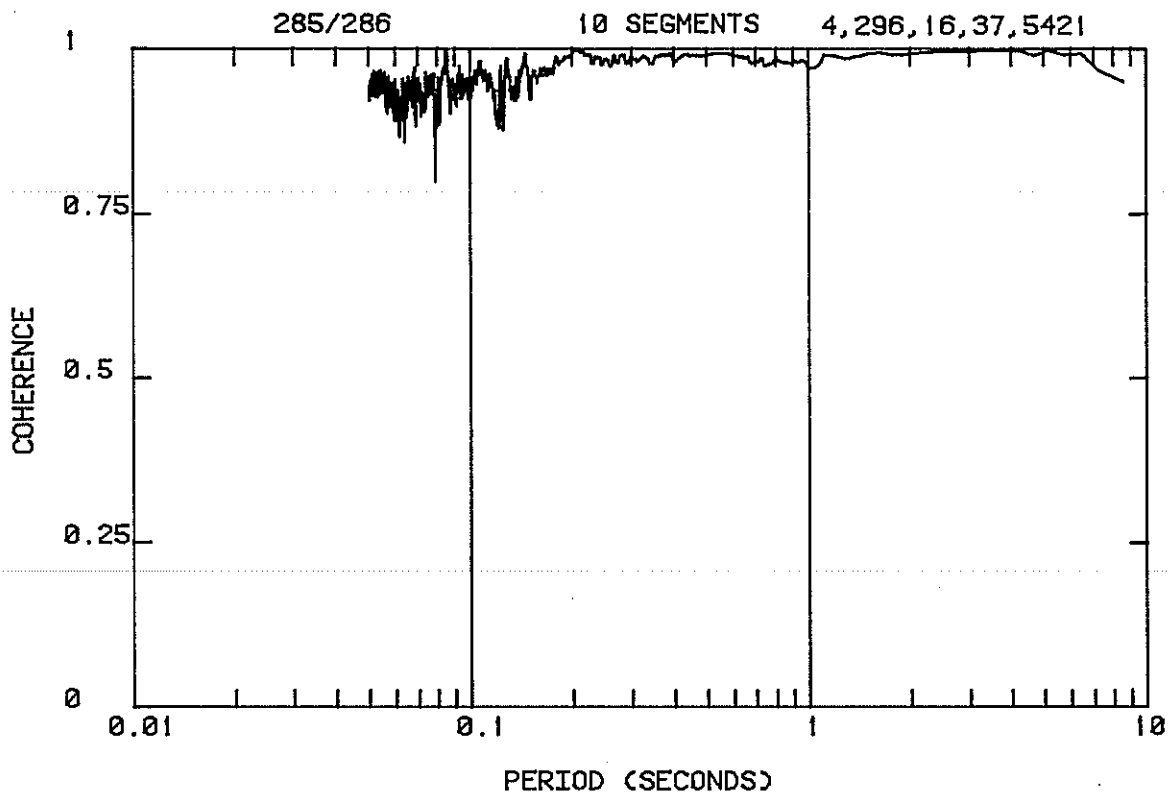

Figure 15.--Coherence between signals taken from two DJ-1 vertical seismometers during a daytime period.

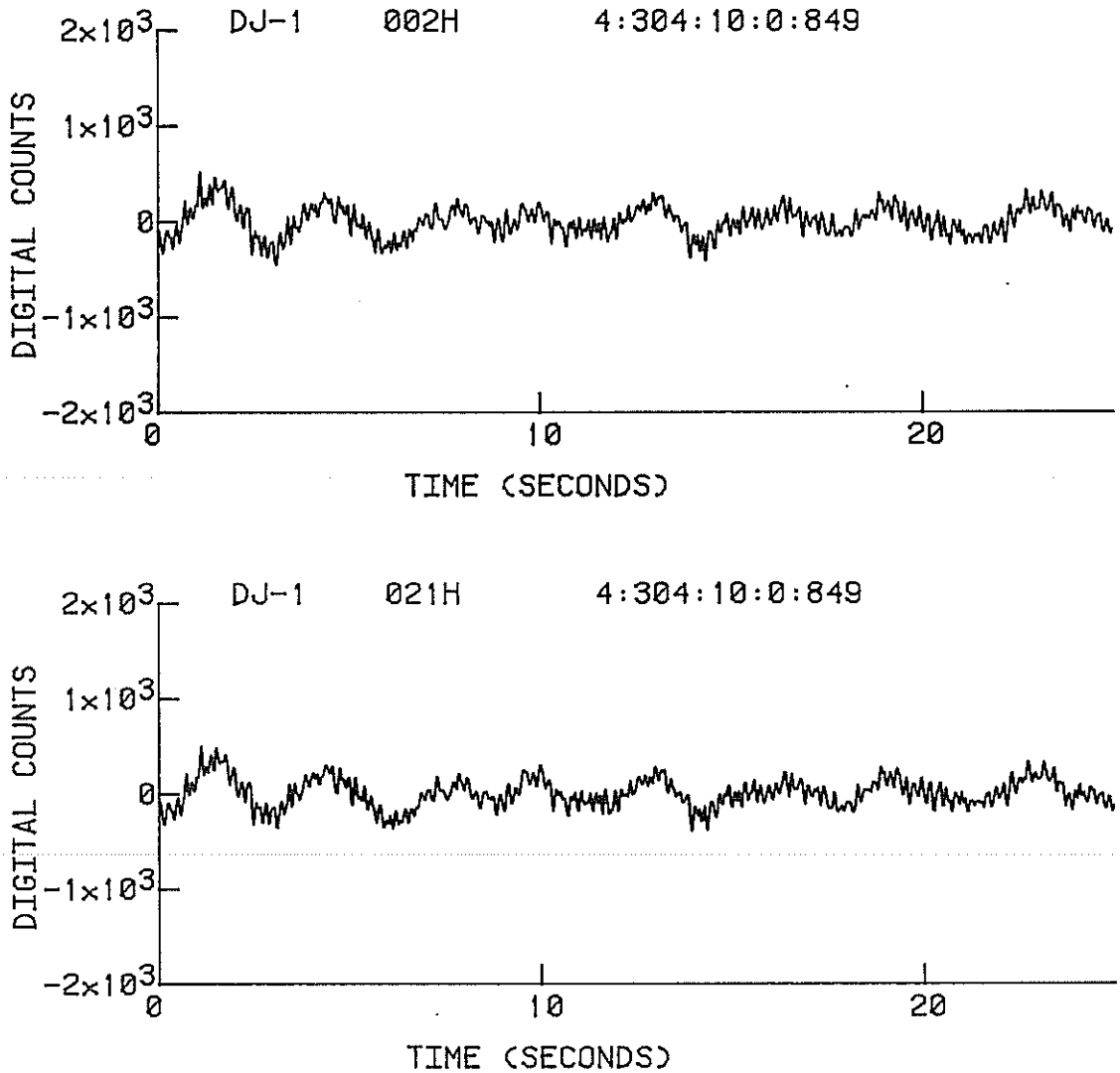

Figure 16.--Sample signal waveforms taken from two DJ-1 horizontal seismometers operated in parallel during quiet nighttime hours.

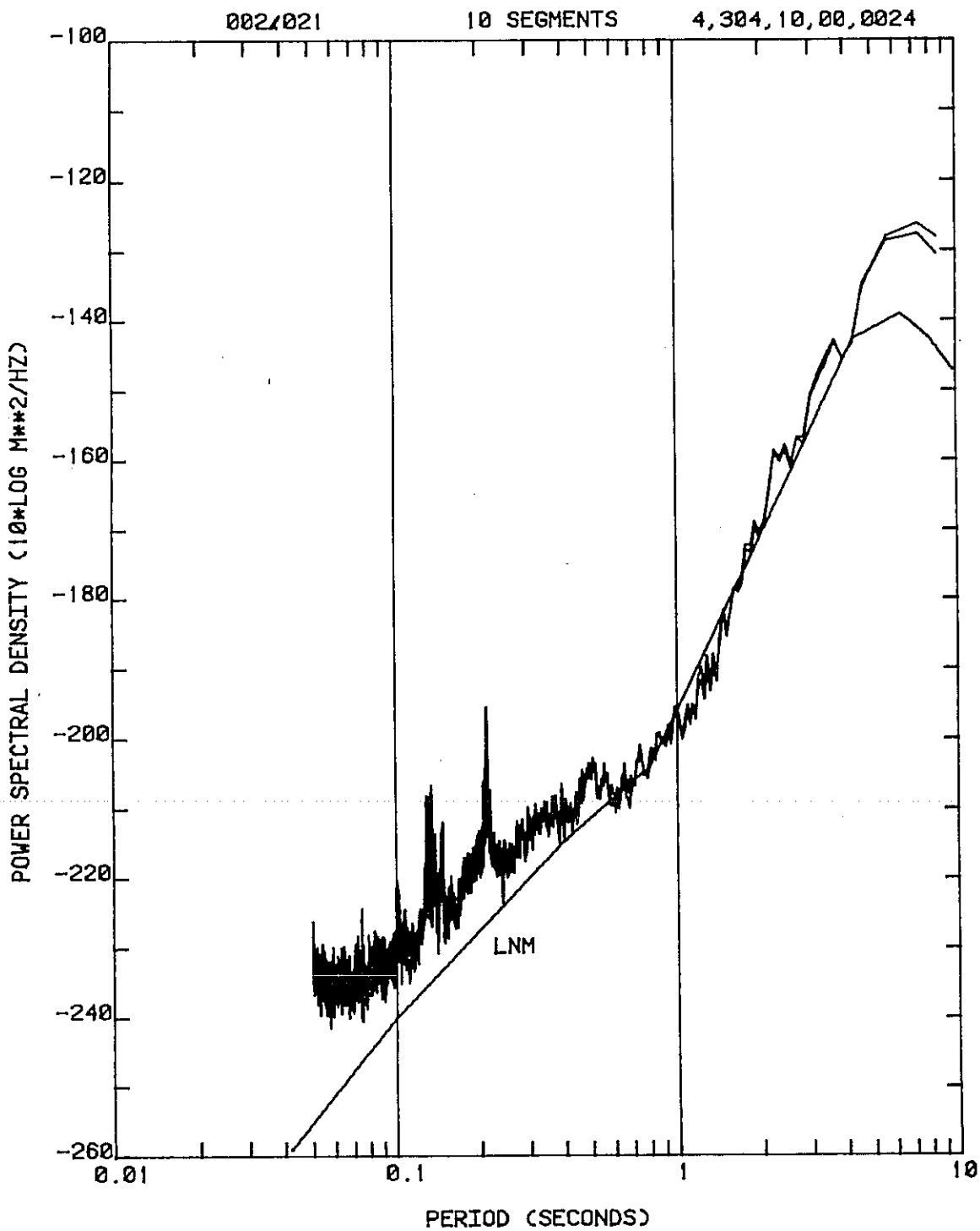

Figure 17.--Power spectral densities computed from signals taken from two horizontal DJ-1 seismometers operated in parallel during a quiet nighttime period.

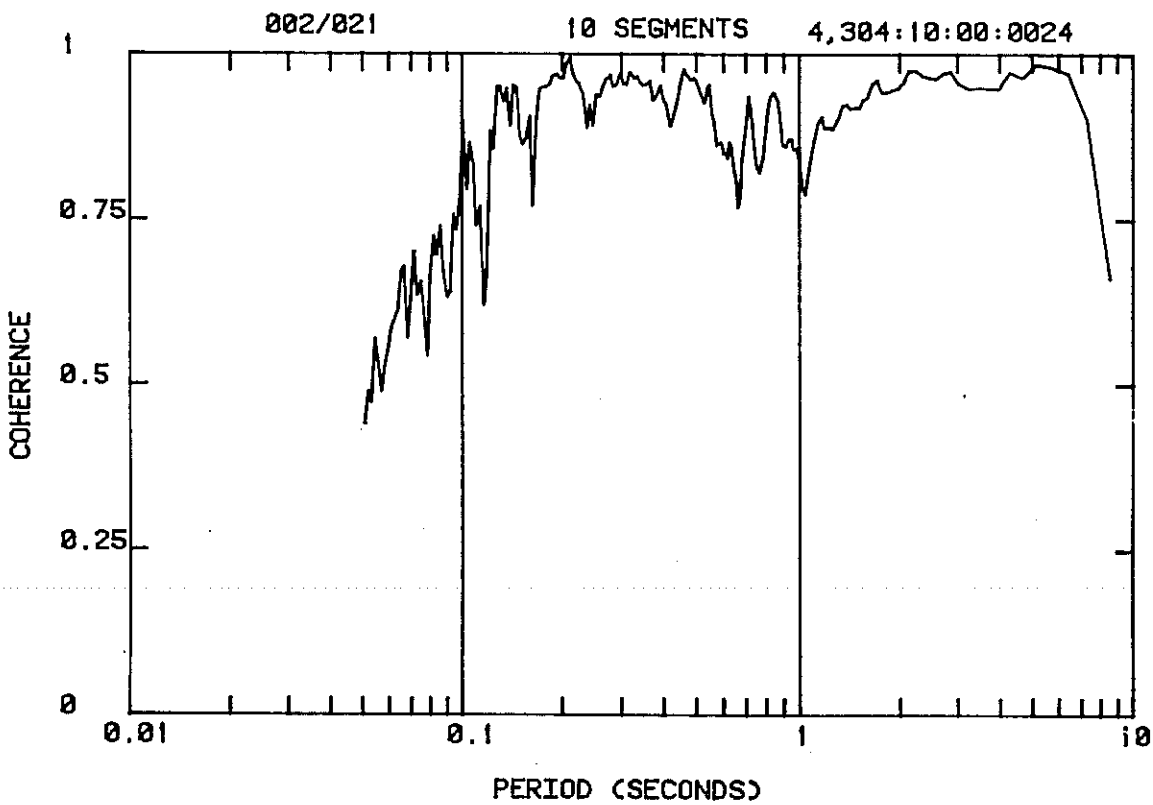

Figure 18.--Coherence between signals taken from two DJ-1 horizontal seismometers during a quiet period.

3. BROADBAND SENSOR SYSTEM

3.1 Introduction

The broadband sensor system chosen for the CDSN consists of a triaxial set of Streckeisen STS-1 seismometers and their companion STS-CCU signal conditioning units. The STS-1 seismometers have been described in a publication by Wielandt and Streckeisen (1982); other important information is given in the manuals that accompany the instruments. The signal conditioners shape and amplify, where necessary, the signals generated in the seismometers and provide three principal outputs, BB, LP, and VLP, all of which will be recorded at the CDSN stations. Remote monitoring and adjustment of the seismometer mass position is another important function of the signal conditioner.

A simplified block diagram showing the active elements of the broadband sensor system is provided in Figure 19. The STS seismometers are force-balance pendulum-type instruments having closed loop periods of 20 seconds and damping ratios of .7071. Incorporated into the electronics of each seismometer is the equivalent of a two-pole low-pass filter cornered at 0.2 seconds. The seismometers have two outputs; one, called the BRB output, is proportional to earth velocity between 0.2 and 20 seconds, and the other, called the LP output, is proportional to earth acceleration at periods longer than 20 seconds. The nominal velocity sensitivity of the BRB output is 12,000 volt-seconds per meter, and the nominal acceleration sensitivity of the LP output is 40,000 volt-second^2 per meter. Both values include a line driver gain of five in the seismometer electronics. Actual values vary from instrument to instrument; precise values are furnished on the data sheets that accompany each seismometer. Since the sensitivities are not easily adjustable, no attempt will be made to set the recording sensitivities to a precise standard value.

Absolute calibration of the seismometers is performed at the factory using a tilt table, a procedure that will not be repeated during installation. The factory specified sensitivity will be used to determine the motor constant of the calibration coil. Routine calibration will consist of step function inputs applied at intervals corresponding to the replacement of the tape cartridges (either weekly or biweekly). Its purpose will be to provide the means to monitor any changes in sensor system sensitivity.

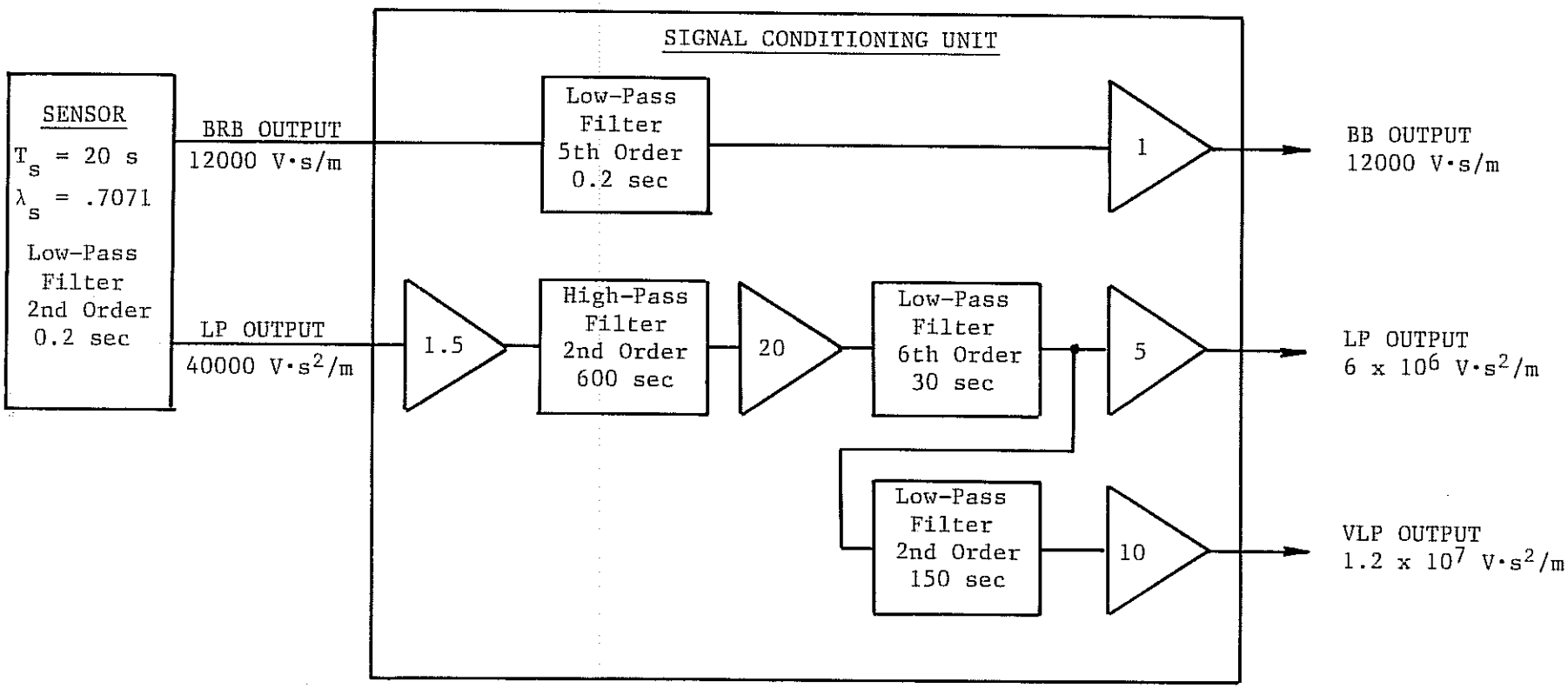

Figure 19.--Simplified block diagram of a CDSN broadband sensor system. Nominal sensitivity values are shown; actual values will vary from instrument to instrument.

3.2 BB Transfer Function

The BRB seismometer output has a response equivalent to the combination of a 20-second seismometer and a two-pole low-pass filter cornered at 0.2 sec. Its transfer function, with respect to earth velocity, can be written as

$$\frac{E_s(s)}{V_e(s)} = \frac{987 \cdot VS \cdot s^2}{(s^2 + .4442s + .0987)(s^2 + 44.42s + 987)} \quad V \cdot s/m$$

where VS is the velocity sensitivity specified for the seismometer (12,000 V·s/m, nominal). In the signal conditioning unit, the BRB signal is converted from differential to single ended and passed through a 5th-order low-pass Butterworth filter. The transfer function of the filter is

$$\frac{E_o(s)}{E_s(s)} = \frac{3.061 \times 10^7}{(s^2 + 50.84s + 987)(s^2 + 19.42s + 987)(s + 31.42)} \quad V/V$$

The final stage in the signal conditioning unit is a fixed-gain buffer amplifier with a gain of unity. The gain of this stage can be changed, if necessary.

Letting BBTF(s) represent the transfer function of the BB channel (digital output of the encoder as a function of earth velocity),

$$BBTF(s) = K_{adc} \cdot \frac{E_s(s)}{V_e(s)} \cdot \frac{E_o(s)}{E_s(s)} \quad DC \cdot s/m$$

where $K_{adc} = 1 \times 10^5$ digital counts per volt. For a seismometer with nominal output sensitivity, the BB velocity sensitivity at midband is $K_{adc} \times VS = 1.2 \times 10^9$ DC·s/m, and the displacement sensitivity at 1 second will be 7.54×10^9 DC/m, or 7,540 DC/micron. The poles and zeros of the broadband transfer function are listed in Table 4. The relative amplitude response and the phase response of the BB channel are shown in Figure 20. The points on the amplitude response curve represent the average of three measured values. Both computed and measured step responses are shown in Figure 21.

Poles	Zeros
-.2221 + j(.2221)	-0.000 + j(0.000)
-.2221 - j(.2221)	-0.000 + j(0.000)
-19.57 + j(24.57)	
-19.57 - j(24.57)	
-25.42 + j(18.47)	
-25.42 - j(18.47)	
-9.708 + j(29.88)	
-9.708 - j(29.88)	
-31.42 + j(00.00)	

Table 4.--BB transfer function poles and zeros for an input of earth velocity.

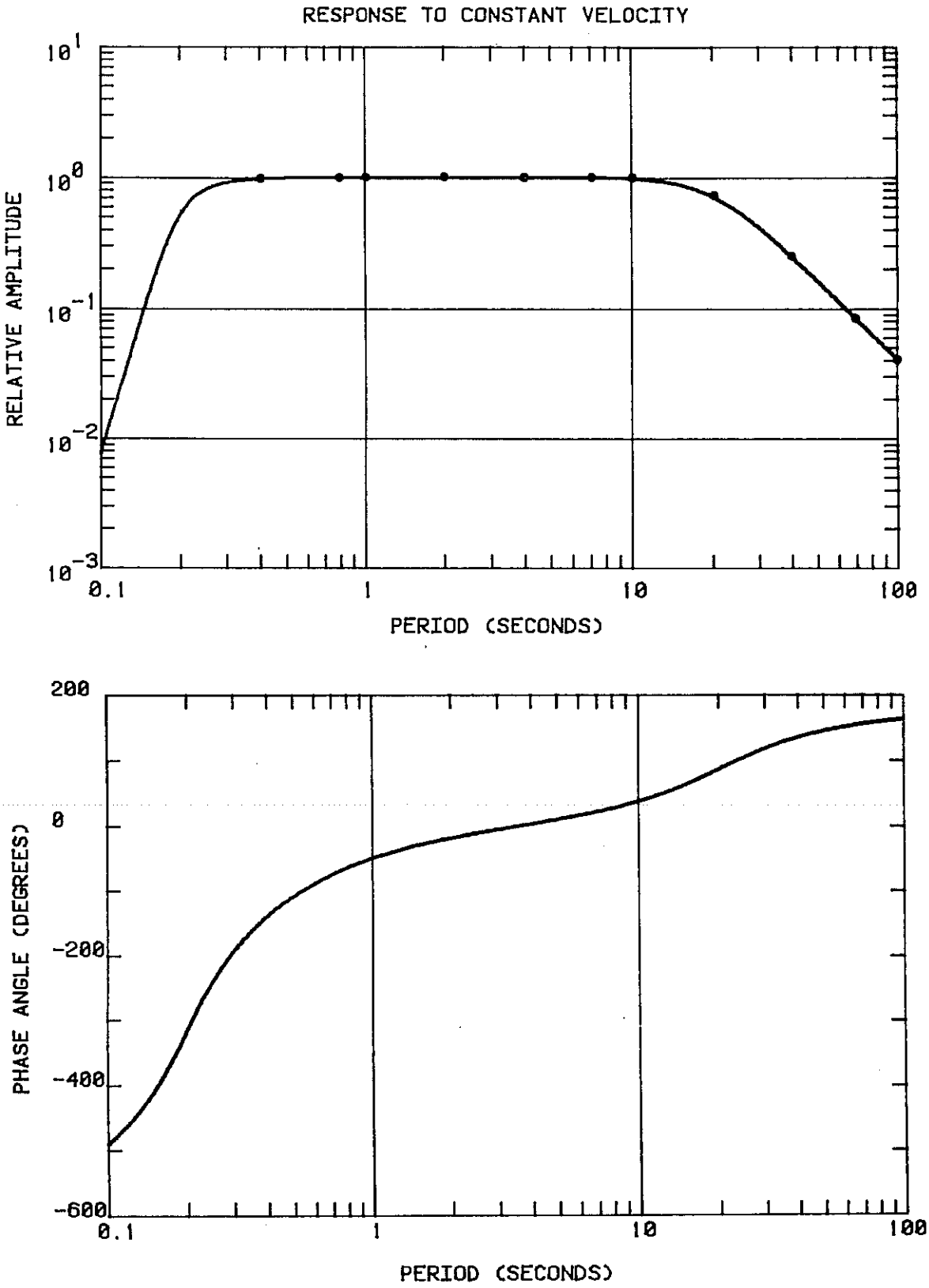

Figure 20.--Amplitude and phase response of the BB channel output of the broadband sensor system computed from the transfer function. Points on the amplitude response curve represent average measured values.

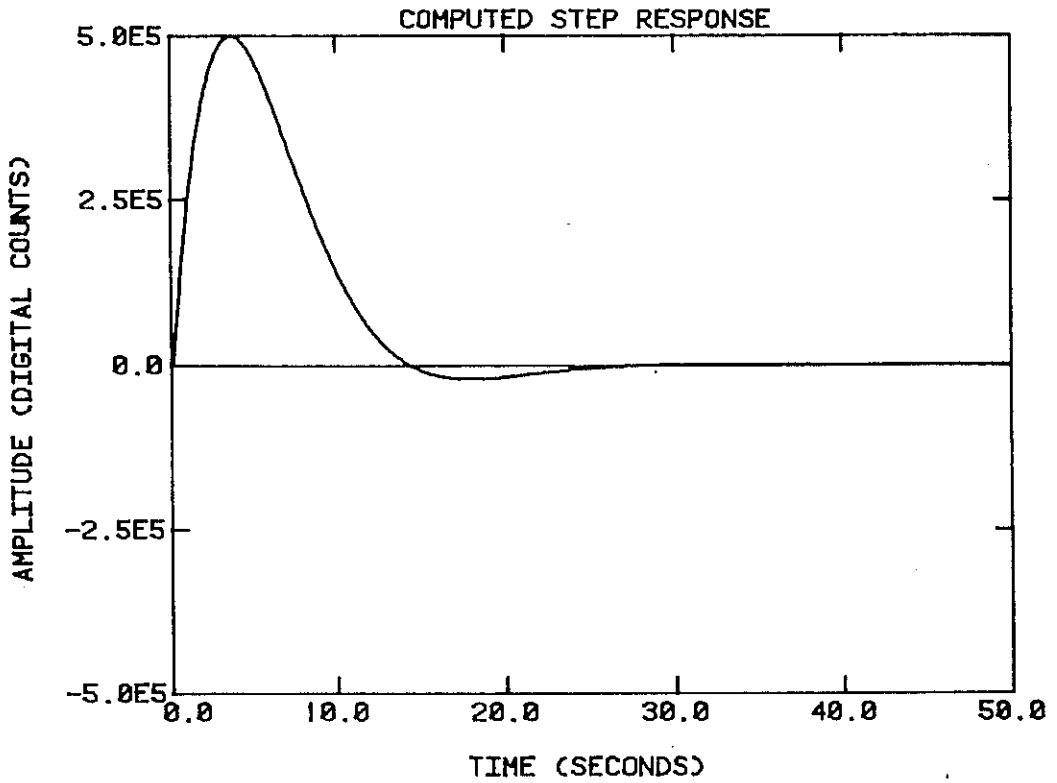

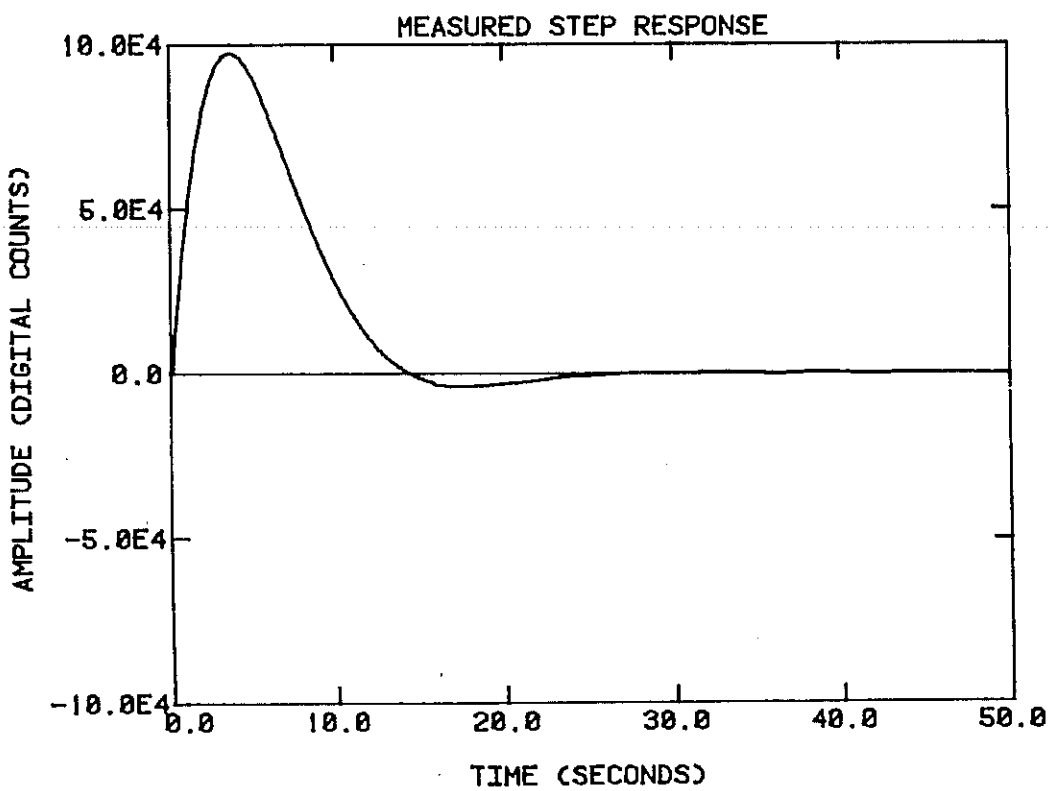

Figure 21.--Examples of computed and measured step resposes for the BB output of the broadband sensor system. In routine operation the amplitude of the step response will be 5 times the amplitude of the measured example to achieve a good signal-to-noise ratio.

3.3 LP Transfer Function

The long-period output of the STS-1 seismometer has a response equivalent to the mass displacement of a 20-second pendulum, that is, proportional to earth acceleration at periods longer than the natural period of the pendulum. The transfer function at the output of the seismometer electronics is

$$\frac{E_s(s)}{A(s)} = \frac{AS}{s^2 + .4442s + .0987} \quad V \cdot s^2/m$$

where A(s) represents earth acceleration and AS is the acceleration sensitivity of the seismometer (40,000 $V \cdot s^2/m$, nominal).

In the signal conditioning unit the seismometer signal is passed through a 2nd-order high-pass filter cornered at 600 seconds and a 6th-order low-pass filter cornered at 30 seconds. The filters have a voltage gain of 30 and there is an additional gain of 5 in the output stage. The transfer function of the filters is

$$\frac{E_o(s)}{E_s(s)} = \frac{150\ s^2}{s^2 + .01481s + .0001097} \cdot \frac{8.437 \times 10^{-5}}{(s^2+.4046s+.04386)(s^2+.2962s+.04386)(s^2+.1084s+.04386)} \quad V/V$$

Letting LPTF(s) represent the transfer function of the LP channel (digital output of the encoder as a function of earth acceleration),

$$LPTF(s) = K_{adc} \cdot \frac{E_s(s)}{A(s)} \cdot \frac{E_o(s)}{E_s(s)} \quad DC \cdot s^2/m$$

For nominal seismometer sensitivity, the digital acceleration sensitivity at midband ($AS \cdot 150 \cdot K_{adc}$) will be 6×10^{11} $DC \cdot s^2/m$, and the displacement sensitivity at 25 seconds period will be 1×10^{10} DC/m, or 10,000 digital counts per micron. The poles and zeros of the LP transfer function are listed in Table 5. The relative amplitude response and the phase response of the LP channel are shown in Figure 22. The points on the amplitude response curve represent the average of three measured values.

Poles	Zeros
-.222100 + j(.222100)	
-.222100 - j(.222100)	
-.007405 + j(.007405)	-.000000 + j(.000000)
-.007405 - j(.007405)	-.000000 + j(.000000)
-.202300 + j(.054200)	
-.202300 - j(.054200)	
-.148100 + j(.148100)	
-.148100 - j(.148100)	
-.054200 + j(.202300)	
-.054200 - j(.202300)	

Table 5.--LP transfer function poles and zeros for an input of earth acceleration.

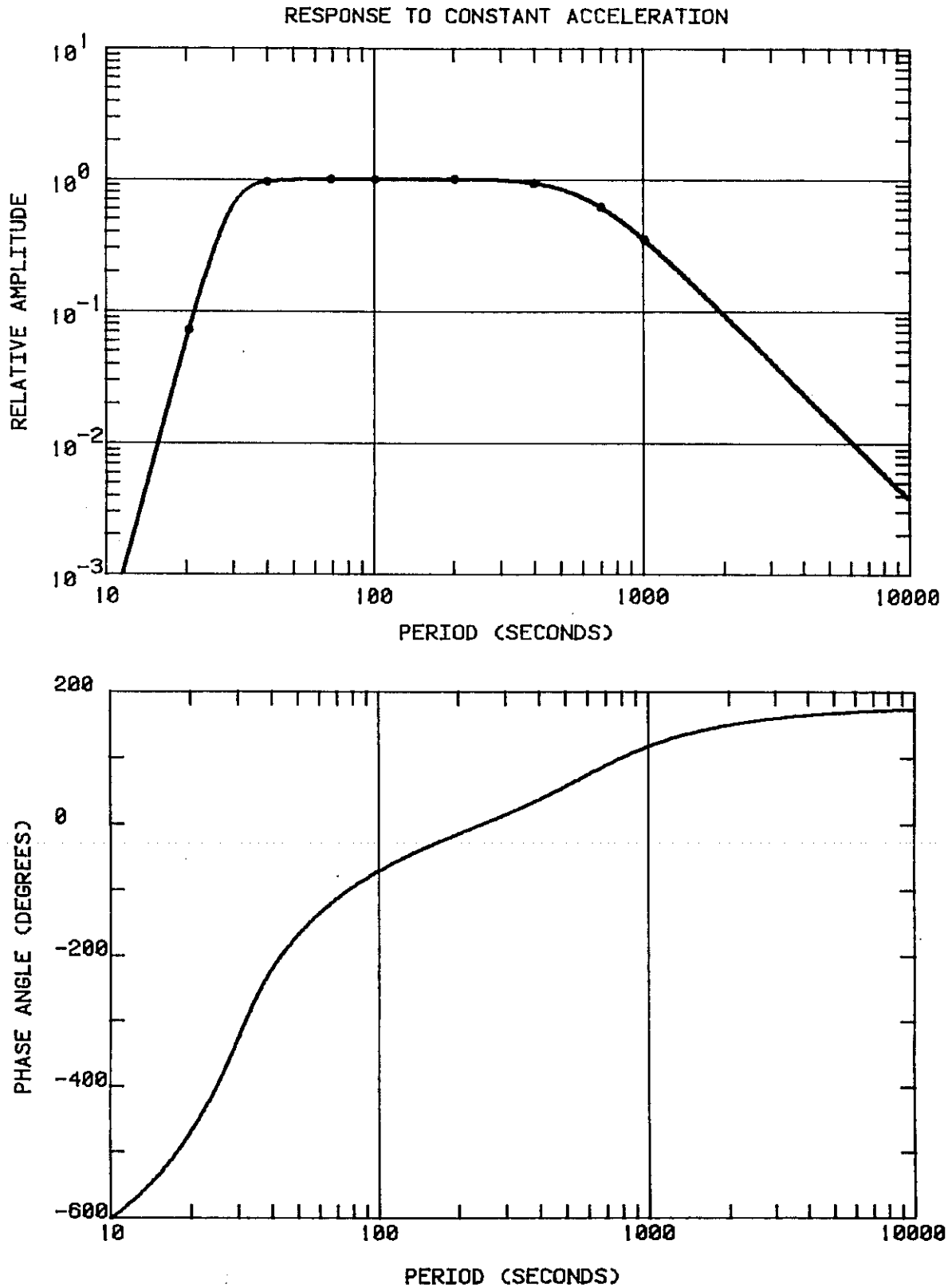

Figure 22.--Amplitude and phase responses of the LP channel output of the broadband sensor system computed from the transfer function. Points on the amplitude response curve represent average measured values.

3.4 VLP Transfer Function

The VLP signal is derived from the LP channel in the signal conditioning unit (see Figure 19), then passed through a 2nd-order low-pass filter cornered at 150 seconds to attenuate the signal at the longer Nyquist period. The output stage has a gain of 10 rather than the gain of 5 used in the LP channel. The transfer function for the VLP channel may be written as follows

$$VLPTF(s) = LPTF(s) \cdot \frac{.00351}{s^2 + .05924s + .001755} \quad DC \cdot s^2/m$$

The poles and zeros of the VLP transfer function are listed in Table 6. The relative amplitude response and the phase response of the VLP channel are illustrated in Figure 23.

3.5 Operational Tests

The primary goals in testing the broadband sensor system were to evaluate installation techniques and to determine levels of background noise that can be expected in a good operating environment. In China, the broadband sensor systems will be installed in surface or shallow subsurface vaults. Noise that results from vault deformation due to pressure loading and other disturbances cannot be avoided. However, the noise that results from barometric and thermal disturbances acting directly on the seismometers can be minimized with careful and well designed installation procedures.

The STS-1 seismometers are relatively small, especially in comparison with older long-period seismometers, so they are easier to protect. The seismometers are furnished with an assortment of installation accessories. These include an outer aluminum cover, a permalloy shield for the vertical component, a vacuum bell jar, and a glass plate (see Figure 24). An aluminum plate is cemented to the center of the glass plate to provide good thermal contact for the seismometer. Silicone rubber on the outer part of the glass plate provides a seal for the bell jar and cable access. In a later version that will be used in China but was not available for testing, a metal ring is attached to the glass plate and provides a cable feed, vacuum port, and an improved seal for the bell jar. The STS-1 manual suggests additional protective measures: a thermal blanket to cover the bell jar and a styrofoam box to enclose the entire instrument package.

Poles	Zeros
-.222100 + j(.222100)	
-.222100 - j(.222100)	
-.007405 + j(.007405)	-.000000 + j(.000000)
-.007405 - j(.007405)	-.000000 + j(.000000)
-.202300 + j(.054200)	
-.202300 - j(.054200)	
-.148100 + j(.148100)	
-.148100 - j(.148100)	
-.054200 + j(.202300)	
-.054200 - j(.202300)	
-.029620 + j(.029620)	
-.029620 - j(.029620)	

Table 6.--VLP transfer function poles and zeros for an input of earth acceleration.

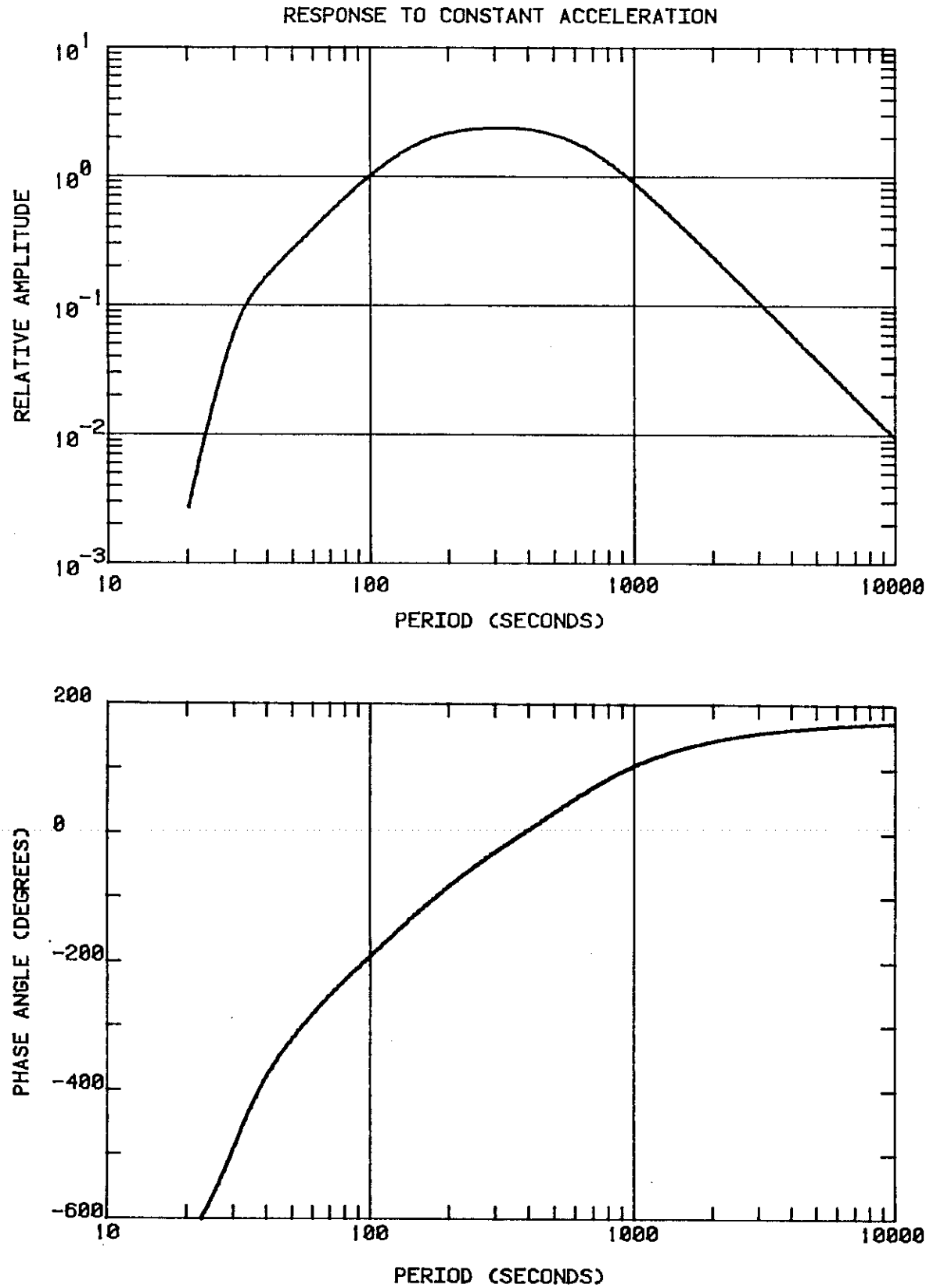

Figure 23.— Amplitude and phase responses of the VLP channel output of the broadband sensor system computed from the transfer function.

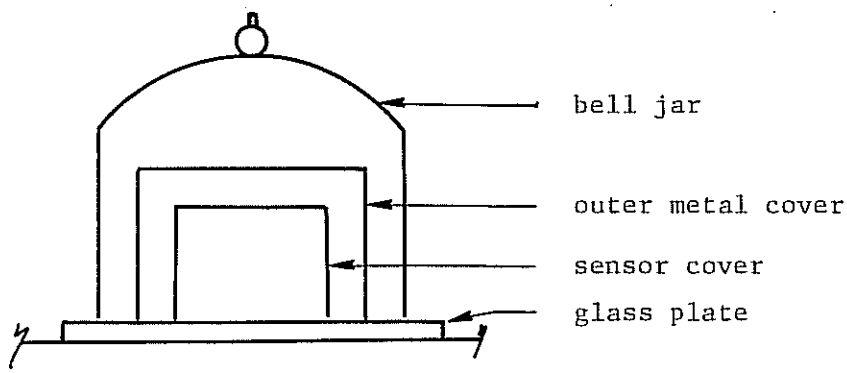

Figure 24.--Illustration of seismometer accessories.

During installation, the bell jars are evacuated sufficiently to form an airtight seal. This eliminates noise in the vertical sensor caused by the response of a buoyant mass to air pressure changes, it may reduce thermal convection, and it protects the sensors from moisture. The glass base plates must be firmly attached to the pier or floor when the bell jars are sealed; otherwise, the base plates may be deformed by pressure changes and this will generate noise, especially in the more tilt sensitive horizontal components. The STS-1 manual suggests using cement for a permanent base plate installation or silicon-based sealant for a temporary base plate installation. The manufacturer suggested further special methods for cementing the plate to the floor and these will be discussed below.

A triaxial set of Streckeisen STS-1 seismographs was installed in a subsurface vault at the Albuquerque Seismological Laboratory with the two horizontal components oriented in an east-west direction. The vault is mined into a granite ridge. The instruments were set up about 15 meters from the entrance and there is about 15 meters of overburden at that location. Temperature variation within the vault normally does not exceed 1^{o} C. Since the CDSN recording system was not available for the tests, the signals were digitized and recorded on a Kinemetrics PDR-2 event recorder. The PDR-2 has a programmable sampling rate and a sensitivity of 105,000 digital counts per volt. Most of the testing involved the analysis of LP signals and these were digitized at a rate of 1 sample per second. Least-count noise power in the LP band, measured by shorting the input to the PDR-2, is shown in Figure 25. The sensitivity of the LP channel

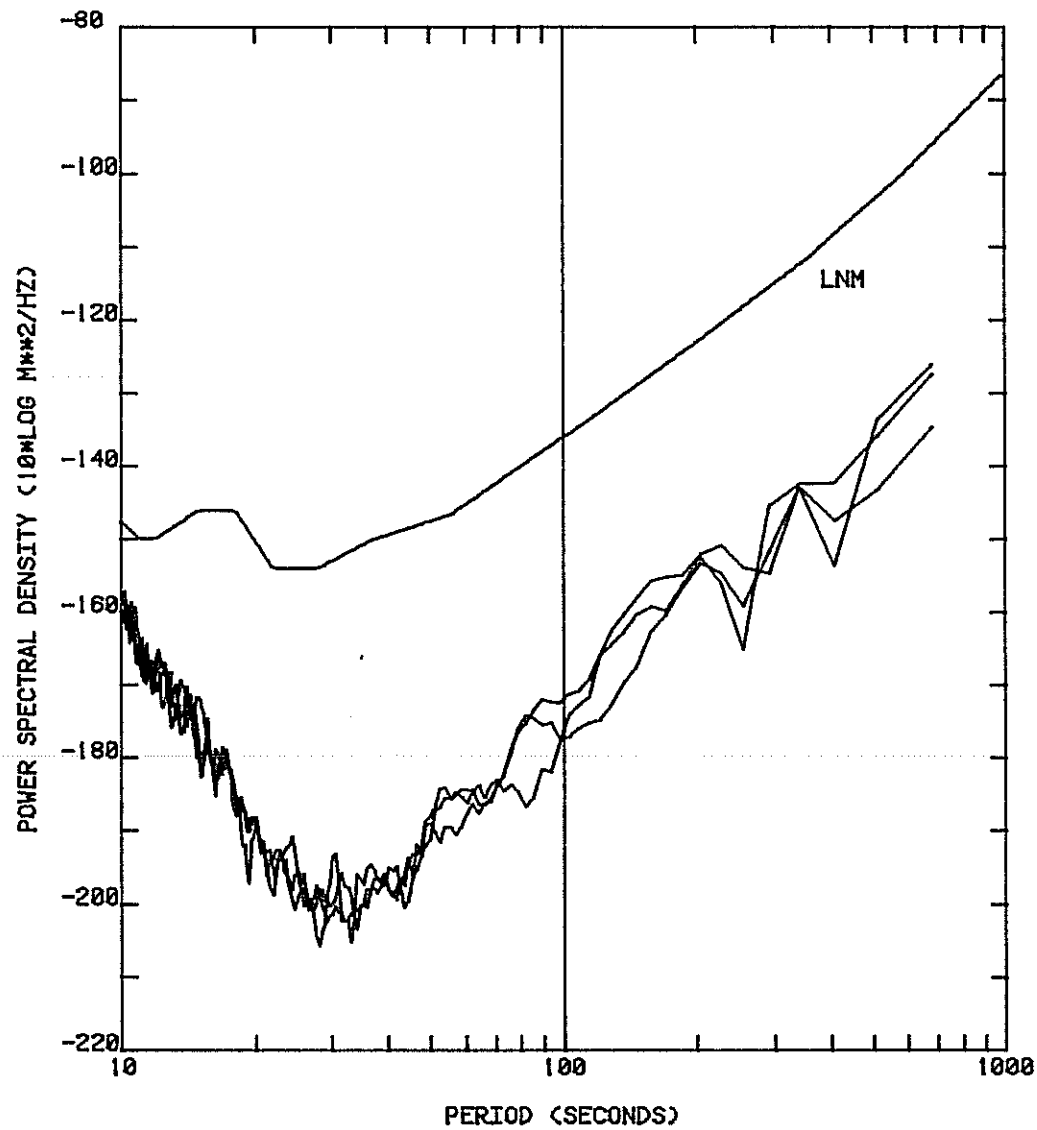

Figure 25.--Least-count noise power measured by shorting the inputs to three PDR-2 channels. Corrected for instrument response. The low-noise model (LNM) for this period range is shown for comparison.

is such that the least-count noise is well below earth background noise for the tests.

The vertical-component sensor was installed by attaching the glass plate to the floor of the vault with a bead of silicon sealant. Then the bell jar was partially evacuated. One of the horizontal sensors (E1) was placed on a glass plate without cementing the plate to the floor. The bell jar was left unsealed, as previous tests have shown that significant noise is generated when the bell jar is evacuated with the plate unattached to the floor (L.G. Holcomb, personal communication). The second horizontal sensor was cemented to the floor more or less according to the manufacturer's suggestions. A form with dimensions about 5 cm larger than the plate was placed on a roughed-up area of the floor. Portland cement was poured into the form to a depth of about 5 cm, and the glass plate was placed on the wet cement. It sank until the base of the plate was about 2 cm from the floor. A plastic vacuum chamber, constructed for the purpose, was placed over the plate and cement. The chamber was pumped down until air bubbles were no longer drawn from the cement (about an hour). The vacuum chamber was removed and the sensor was installed on the plate. Then the bell jar was placed over the sensor and pumped down for about 5 minutes to flex the plate and left partially evacuated. The cement was allowed to cure for 5 days. All three sensor systems were covered with boxes made from 1-inch-thick styrofoam.

Power spectral densities computed from LP signals taken from the three sensor systems during a quiet (wind-free and event-free) period are shown in Figure 26, together with coherence computed between signals from the two parallel horizontal components. Unless otherwise noted, the power spectral densities are averaged from ten 2048-point data segments with approximately a 20% overlap. All are corrected for instrument response. The poor coherence at periods longer than 30 seconds is a clear indication that local effects of the environment, probably thermal convection, are generating excessive noise in the horizontal components. The power levels indicate that the cemented sensor is less noisy than the uncemented sensor, although both are significantly noisier than the vertical component at periods longer than 50 seconds. During a period when the wind speed was about 13 meters per second (30 mph), noise power in the horizontal components rose about 12 dB, as shown in Figure 27, and there was no observable increase in noise from the vertical component. As expected, the coherence

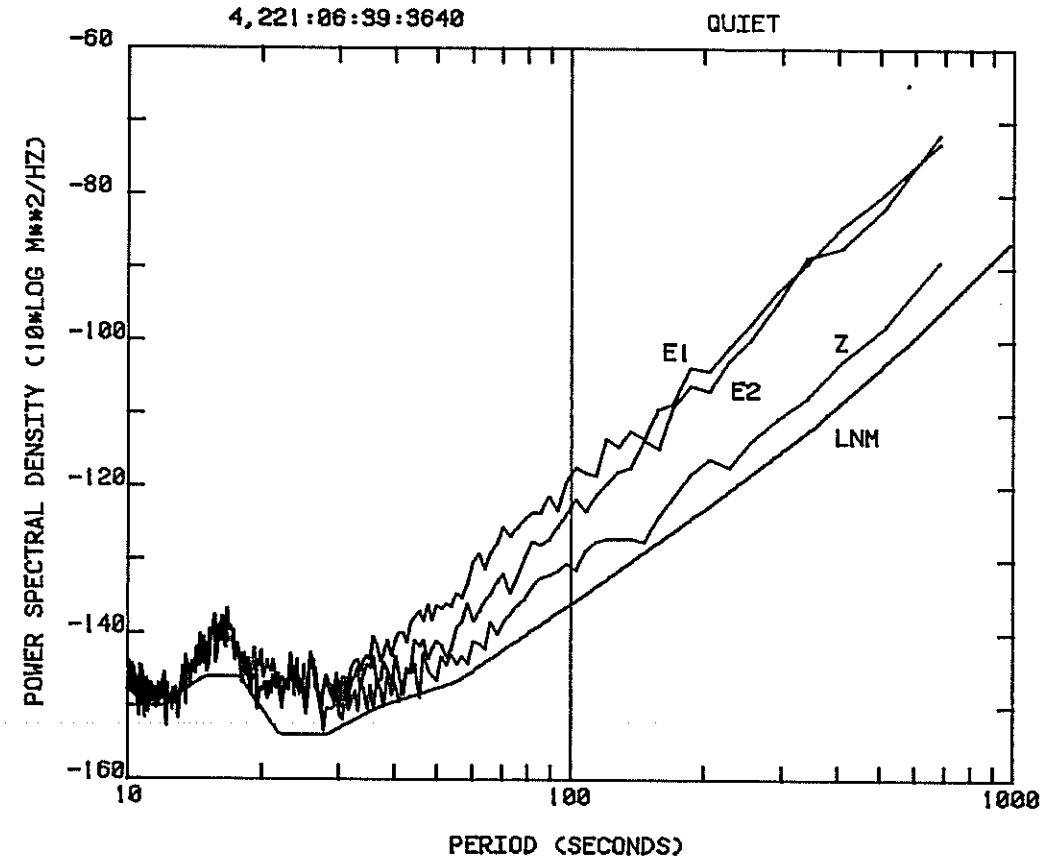

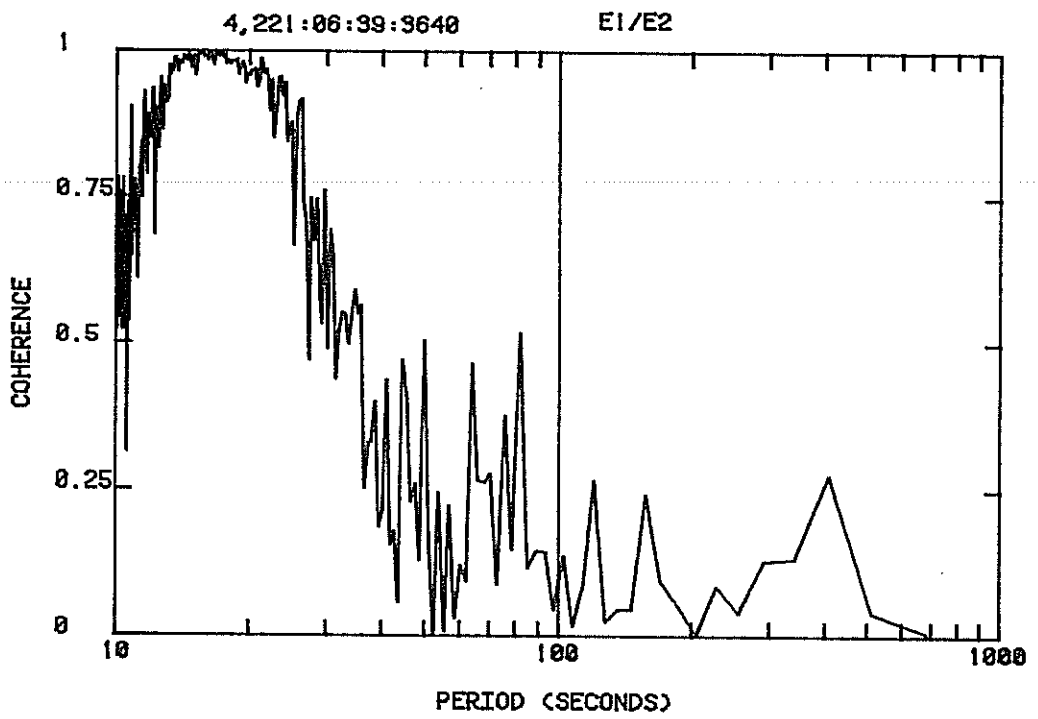

Figure 26.--Power spectral densities (above) computed from LP signals taken from three STS-1 components during a quiet period, and coherence (below) between the two horizontal components. During the test the base plate of E1 was resting freely on the floor and the base plate of E2 was cemented to the floor.

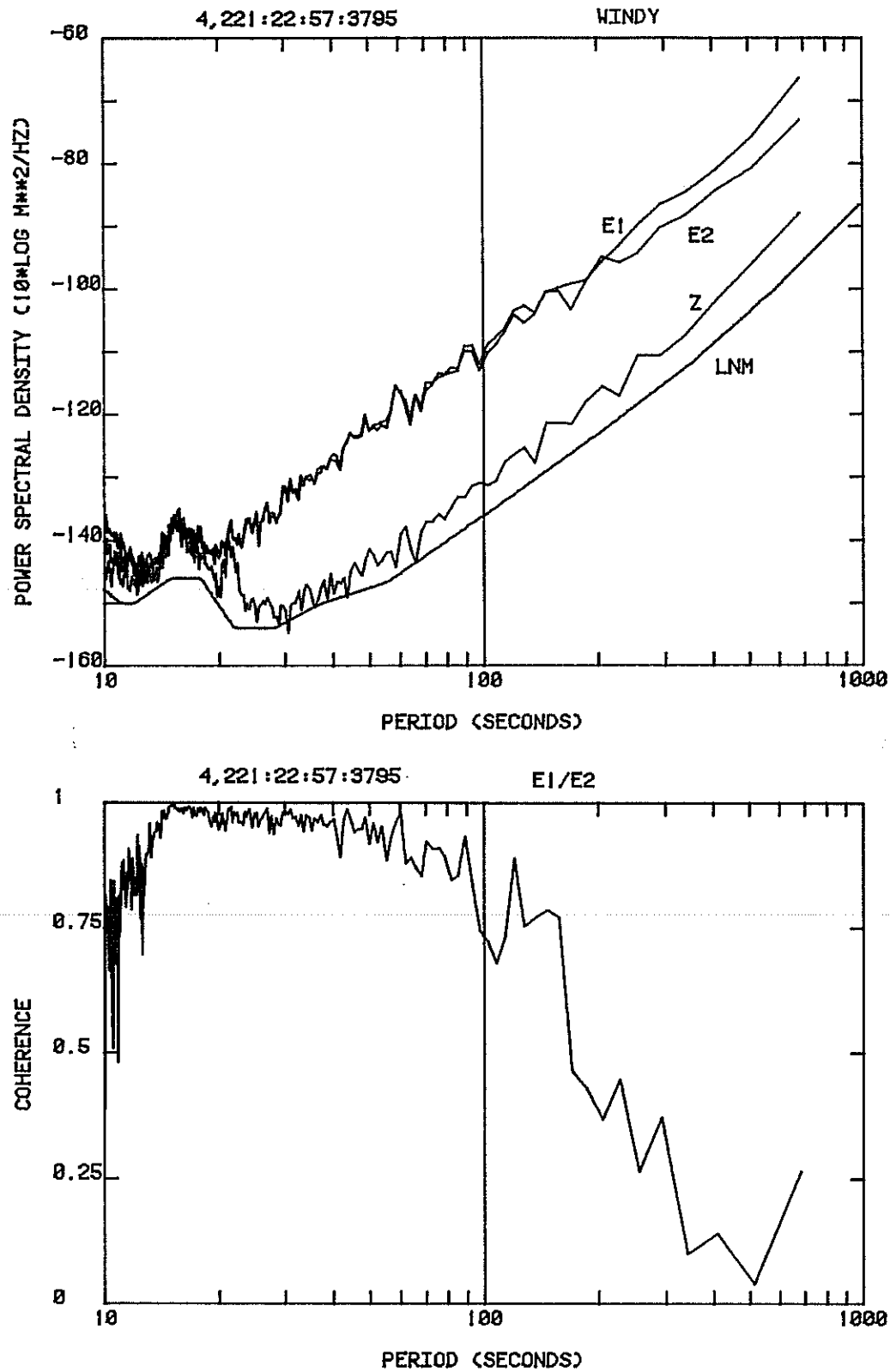

Figure 27.--Power spectral densities (above) computed from LP signals taken from three STS-1 components during a windy period and coherence (below) between the two horizontal components. During the test the base plate of E1 was resting freely on the floor and the base plate of E2 was cemented to the floor.

between the horizontal components is much higher during this period; but the effect of the wind appears to be limited to the period range from 20 to 300 seconds.

For the next test, the glass plate of the component E1 was attached to the floor with a bead of silicon sealant. The bell jar of E2 was partially evacuated, and the bell jar of E1 was removed from the instrument. In an effort to reduce noise caused by thermal disturbances, inner boxes made of styrofoam were placed around the two horizontal components and filled with styrofoam pellets. No changes were made to the vertical-component sensor system. Power spectral densities computed from signals taken from the three components during a quiet period are shown in Figure 28 together with the coherence between signals from the two horizontal components. The coherence is significantly higher compared to the first test data shown in Figure 26. Spectral power and coherence of signals taken during a windy period (wind speed about 9 m/s) are shown in Figure 29. The horizontal sensor attached to the floor with sealant produces about a 4 dB higher power output than the cemented horizontal sensor in response to tilt deformation, although the response to microseisms and events (see Figure 30) is identical for both instruments. The sealant is compliant and would yield in response to a torque produced by the offset center of mass. If this is the cause of the higher sensitivity to tilt deformation, one could expect a much greater effect with the heavy bell jar in place.

It follows from these preliminary test results that the horizontal-component sensor plates must be cemented to the pier to achieve best operational performance and that the sensors should be covered with styrofoam pellets or equally protected in some other way from thermal disturbances. Perhaps the vertical-component data can be marginally improved by these procedures as well, although the vertical sensor clearly does not require the same measure of protection as the horizontal sensor. The installation method that will be used in China for all components is illustrated in Figure 31.

Data from the STS-1 sensor systems were compared with data taken from the ANMO SRO system which is located about 1 km from the vault. The SRO system derives its signals from a KS-36000 borehole seismometer installed at a depth of 100 m. Power spectral densities computed from signals taken from the two vertical-component sensors are shown in Figure 32 for the period range from 10 to 100 seconds and in Figure 33 for the period range from 100 to 10,000 seconds. The comparison is not really meaningful, as the ANMO SRO vertical-component

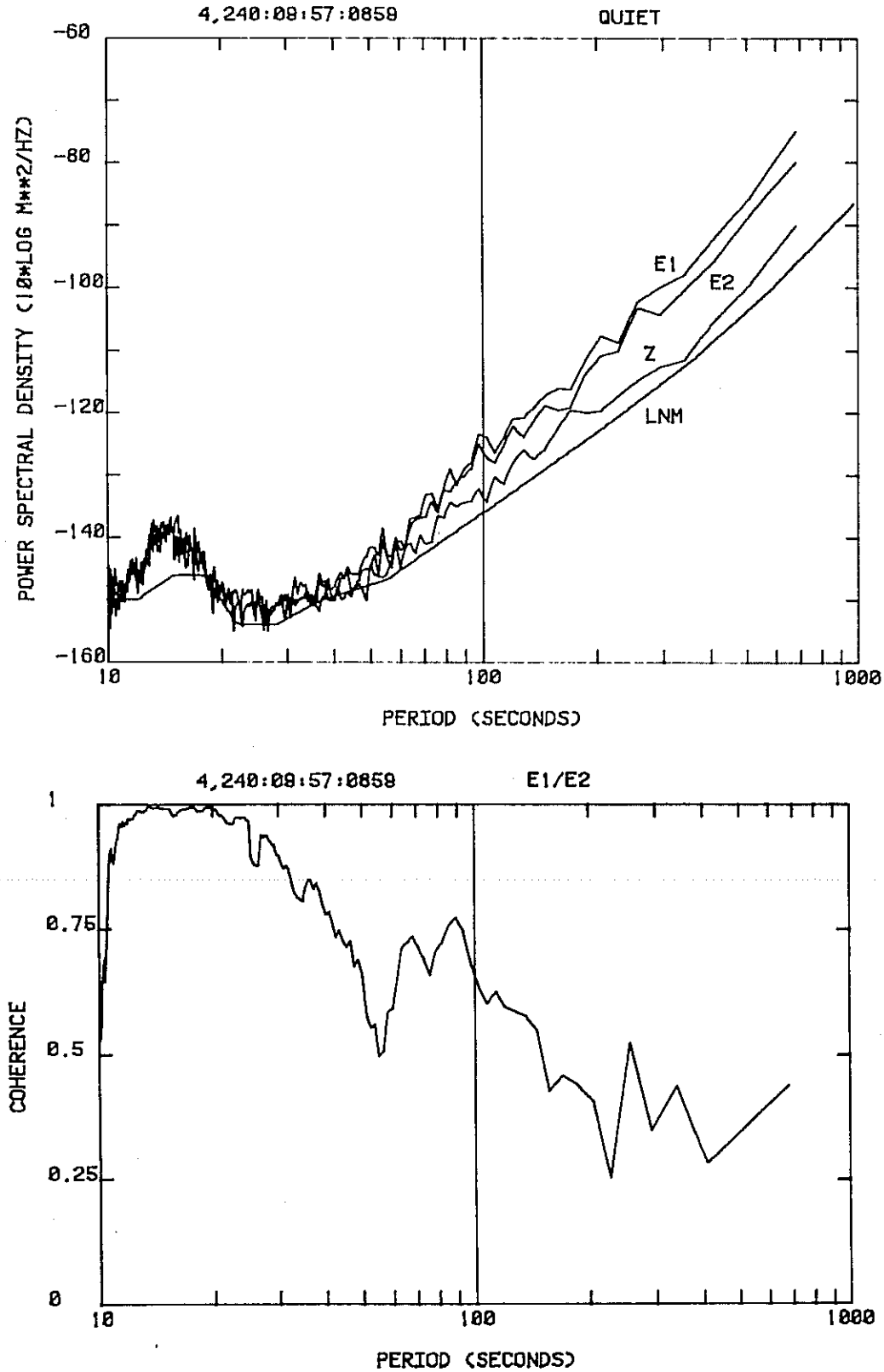

Figure 28.--Power spectral densities (above) computed from signals taken from three STS-1 components during a quiet period and coherence (below) between signals of the horizontal components. Both horizontal sensors were covered with styrofoam pellets; E1 attached with sealant, E2 with cement.

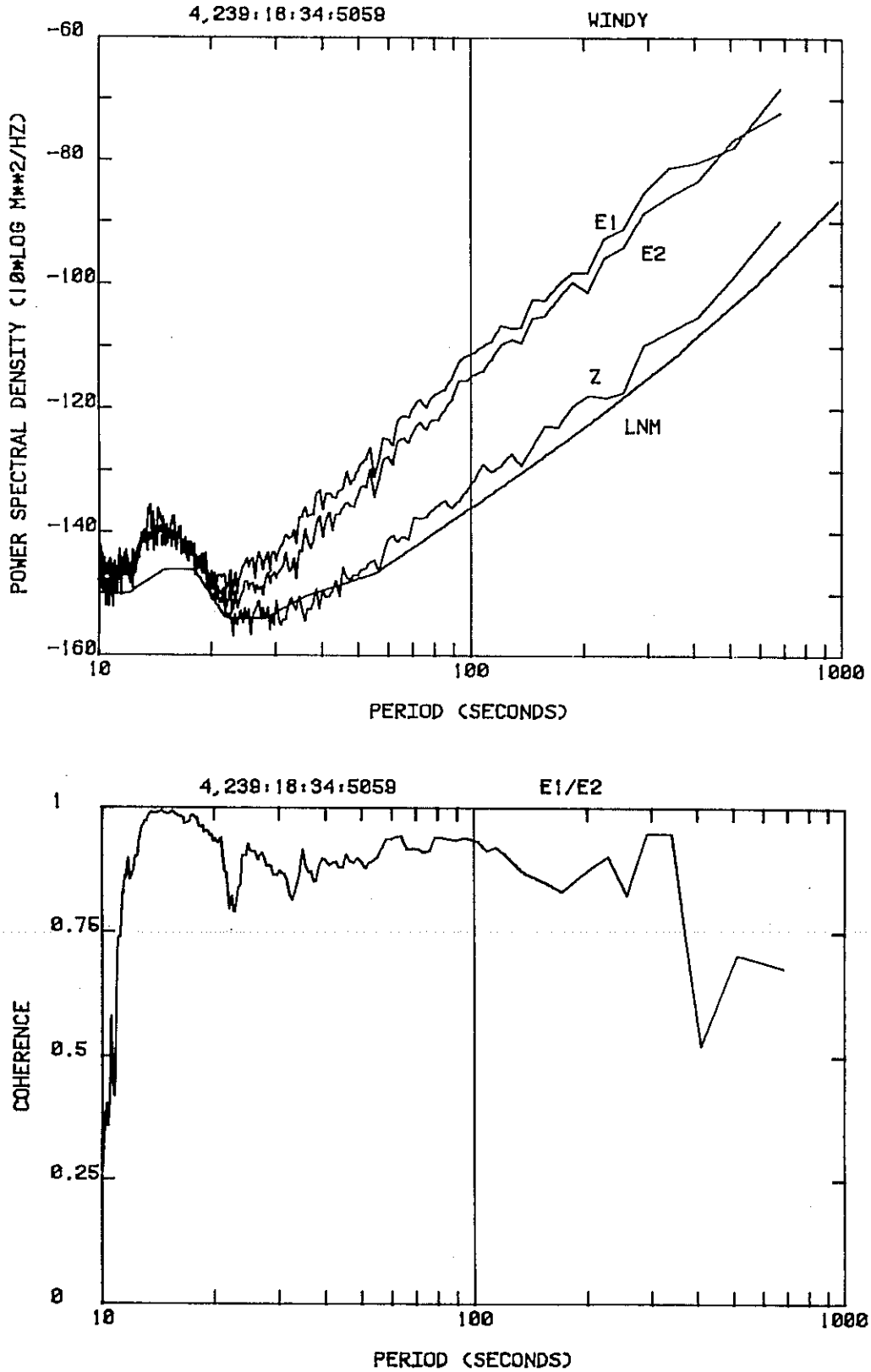

Figure 29.--Power spectral densities (above) computed from signals taken from three STS-1 components during a windy period and coherence (below) between signals of the horizontal components. Horizontal instruments covered with styrofoam pellets; E1 attached with sealant, E2 with cement.

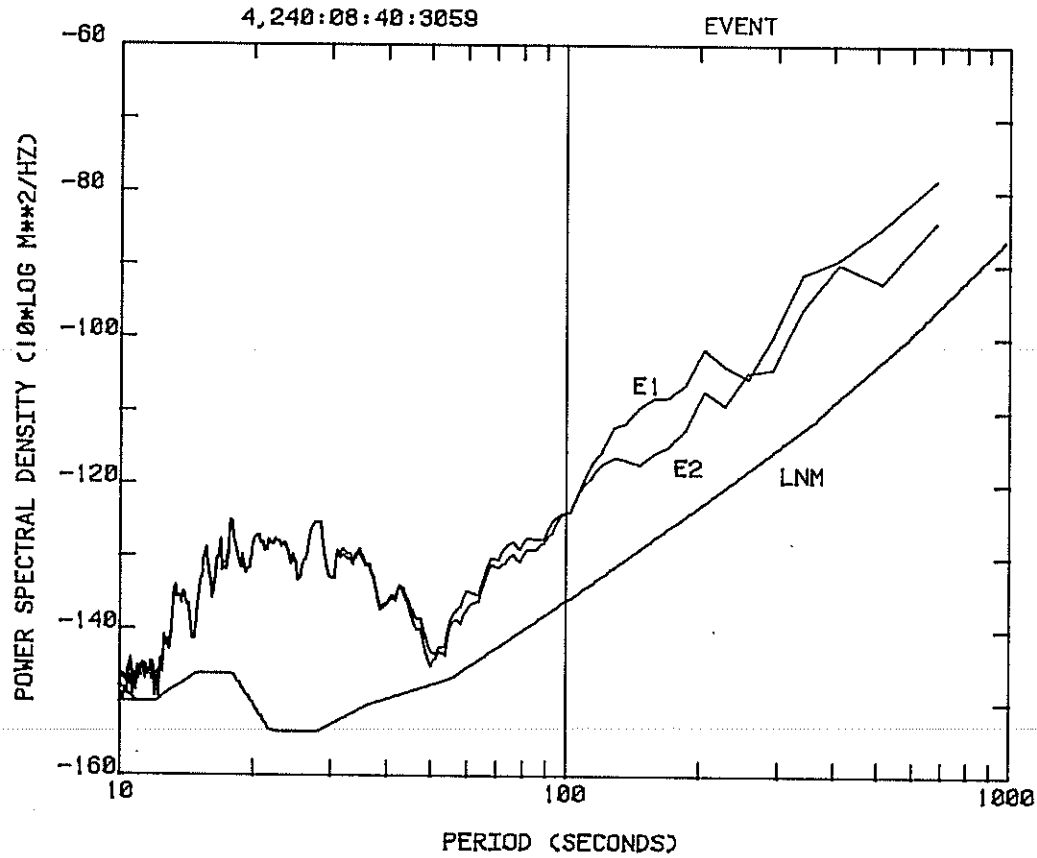

Figure 30.--Power spectral densities of STS-1 horizontal components computed from signals that include surface waves from an earthquake.

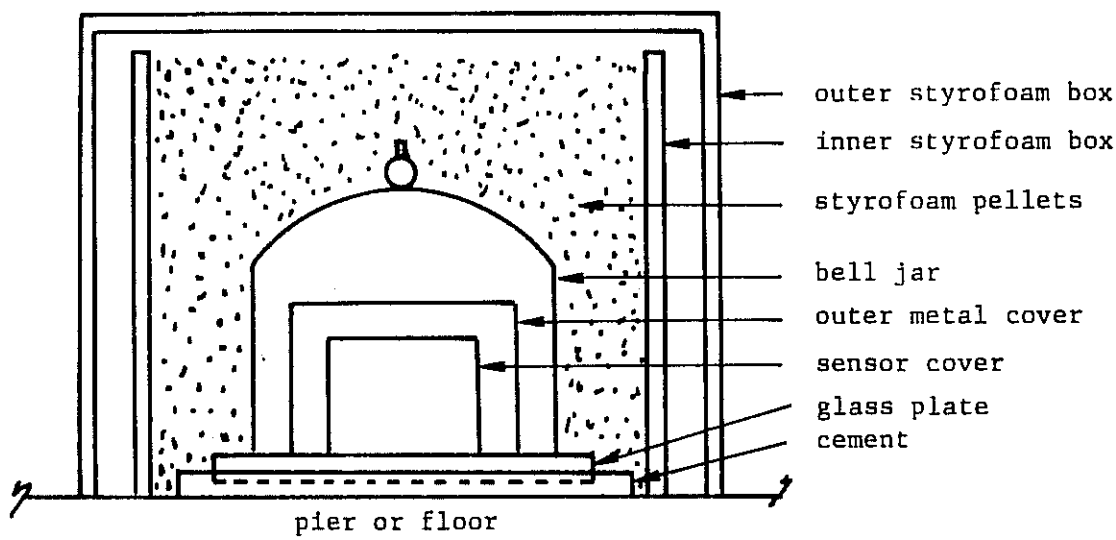

Figure 31.--Illustration of STS-1 installation technique to be used in the CDSN.

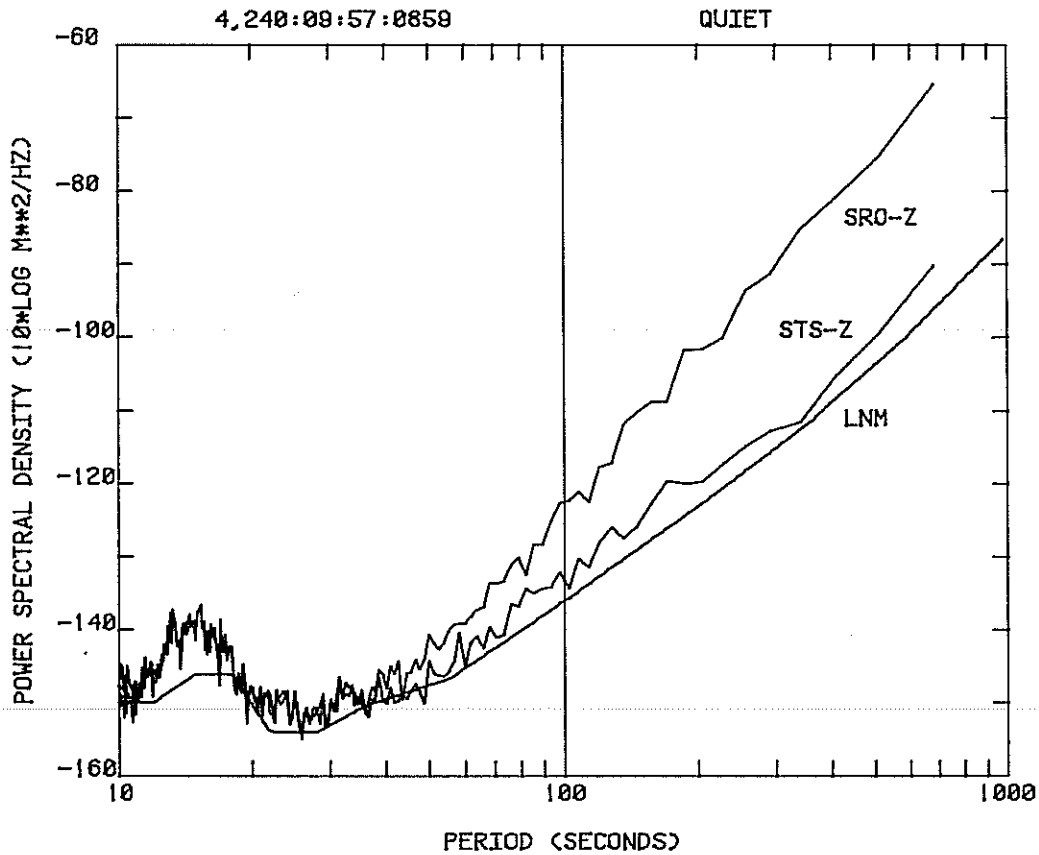

Figure 32.--Power spectral densities computed from signals taken from the STS-1 vertical component and the ANMO SRO vertical component during the same time period.

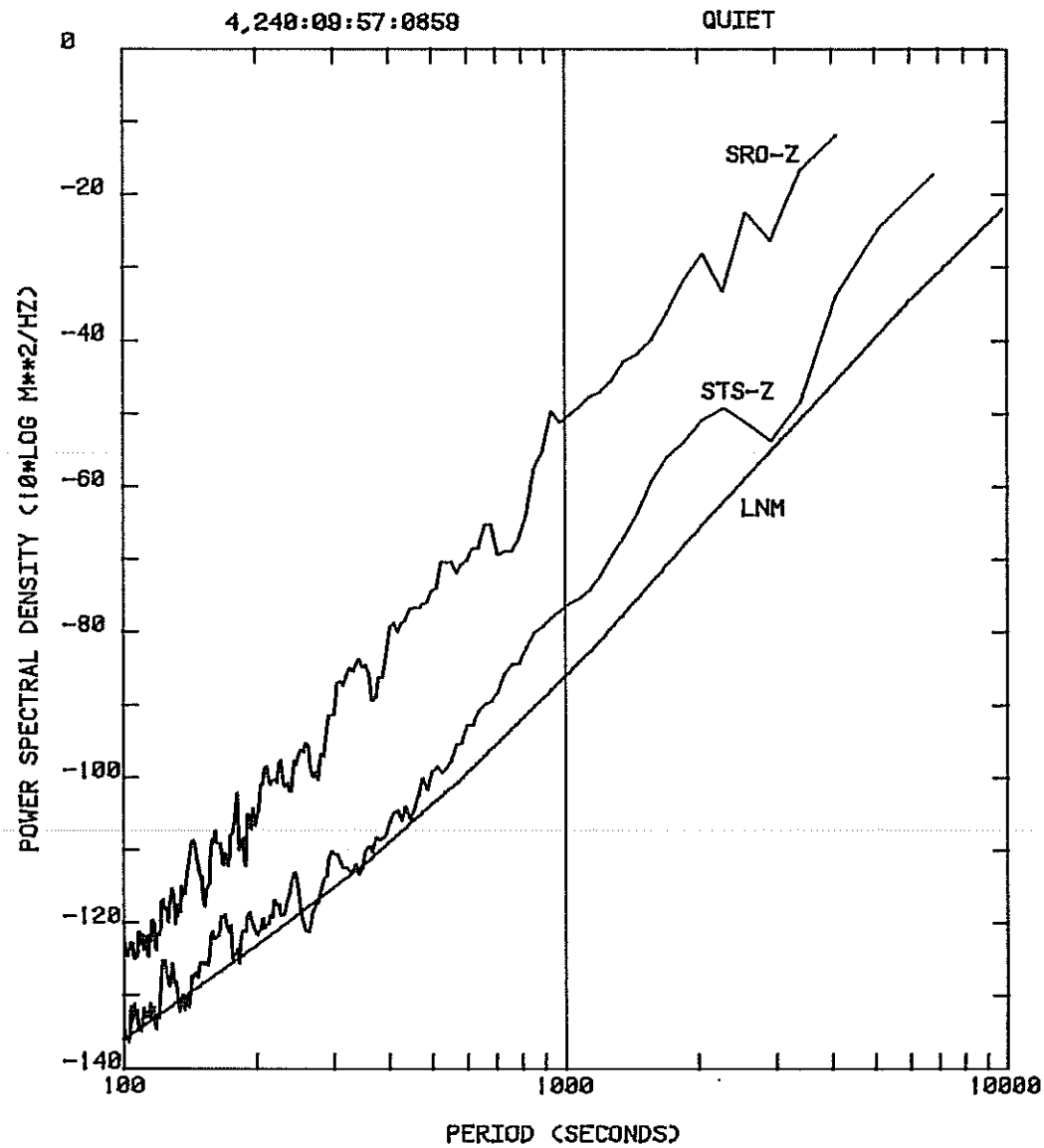

Figure 33.--Power spectral densities computed from signals taken from the STS-1 vertical component and the ANMO SRO vertical component during the same time period.

sensor is known to be abnormally noisy. The cause of the noise is not known, although similar long-period noise in the past has been attributed to a leaking capacitor in the feedback circuit. Test data taken from the horizontal sensors are more meaningful. Power spectral densities are shown in Figures 34 and 35. During a wind-free period, the noise power of the STS-1 and SRO horizontal sensors is about equal in the period range from 10 to 100 seconds; at longer periods the STS-1 sensor is quieter than the SRO sensor. During a windy period (wind speed about 9 m/s), the noise power of the STS-1 horizontal sensor increased about 12 dB relative to the SRO sensor (see Figure 36).

During the tests, distinct signals with periods ranging from 400 to 800 seconds were occasionally observed on the STS-1 analog records. Although they could not be identified on the SRO analog records, the signals were revealed in the SRO data when the digital waveforms were filtered and decimated. Examples are shown in Figure 37. The signals are believed to be caused by infrasonic pressure disturbances of the type described by Bowman and Bedard (1971) and attributed by them to severe weather. They are potentially a significant part of deformation noise in the VLP band.

Data taken from the BB channels of the STS-1 sensor systems were also analyzed to determine background noise levels that can be expected at a quiet site. The results are shown in Figure 38. The spectral data at periods shorter than 10 seconds were obtained by averaging spectral estimates derived from ten 2048-point data segments; spectral data at periods longer than 10 seconds were derived from single 20,480-point segments decimated to 2048 points. At the sensor band edges (0.2 and 20 seconds) least-count noise will be a factor in the signal background, as indicated by the curve labeled PDR-2 in the figure, but this is not an important concern as the design goal for the BB channels is to record moderate-to-large earthquakes.

The STS-1 seismographs are well designed instruments. When properly installed in a good vault, they can be expected to produce high-quality BB, LP, and VLP data. However, the extent of surface deformation that results from atmospheric pressure fluctuations is a function of the rigidity of the rock (Sorrells, 1971). Installation of the STS-1 seismographs on rock less rigid than granite is likely to result in higher noise levels than those observed at the Albuquerque observatory.

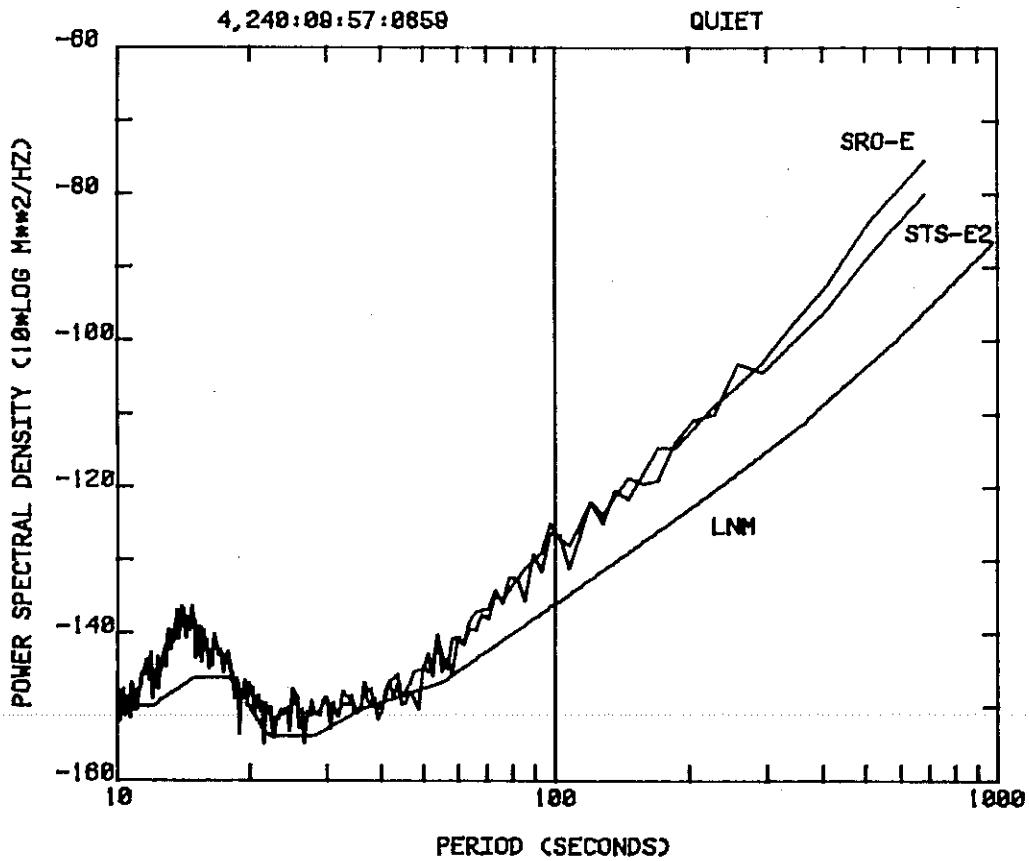

Figure 34.--Power spectral densities computed from signals taken from the STS-1 E2 horizontal component and the ANMO SRO E component during a wind-free period.

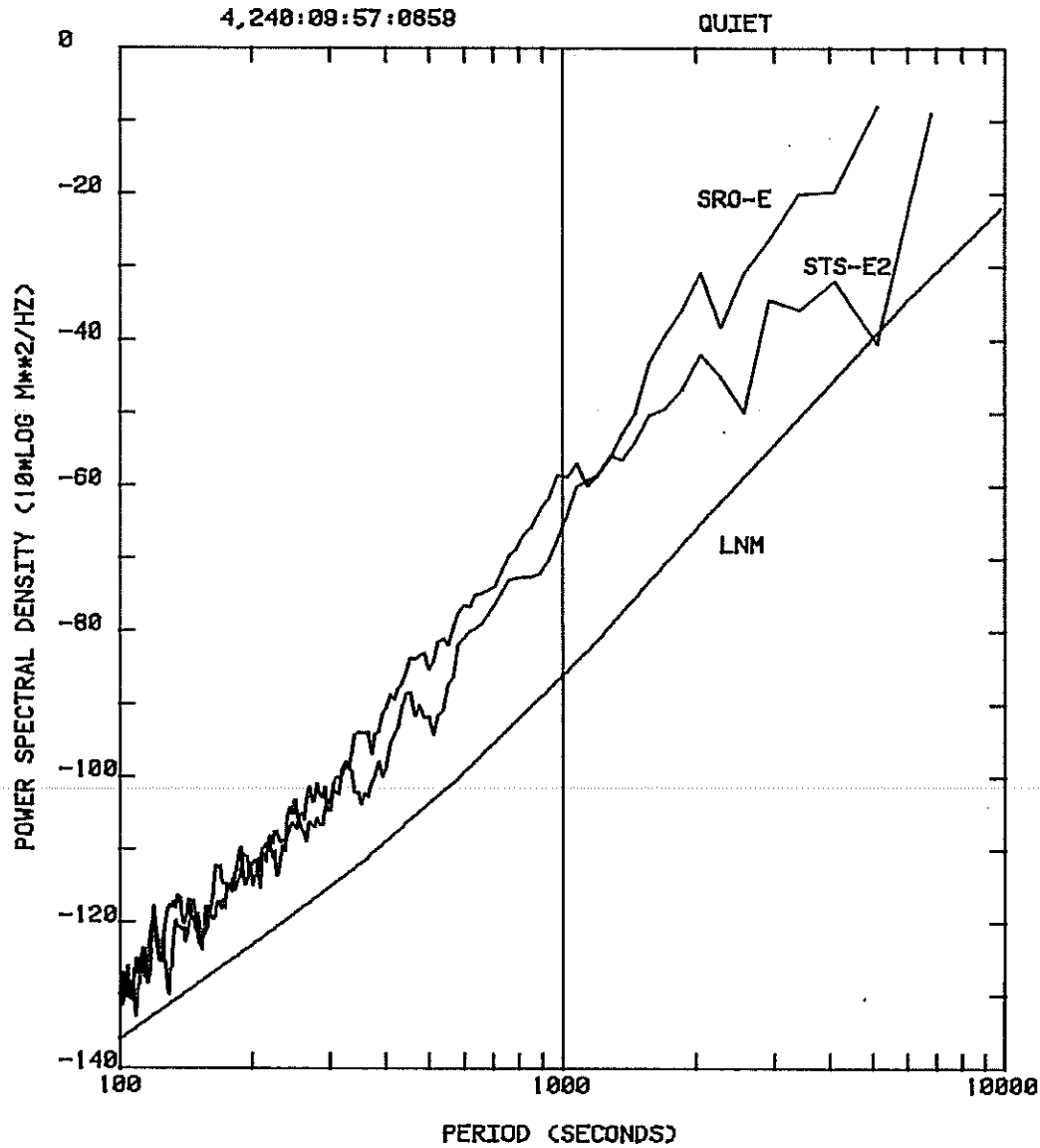

Figure 35.--Power spectral densities computed from signals taken from the STS-1 E2 horizontal component and the ANMO SRO E component during a wind-free period.

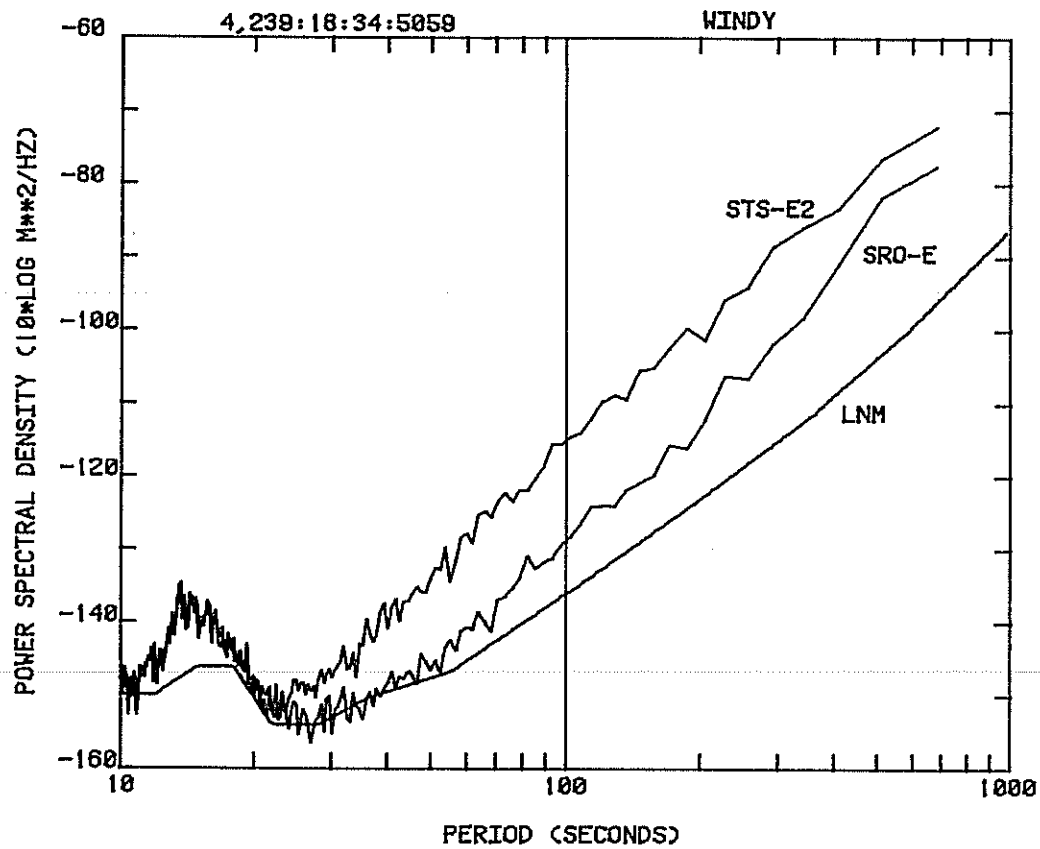

Figure 36.--Power spectral densities computed from signals taken from the STS-1 E2 horizontal component and the ANMO SRO E component during a windy period.

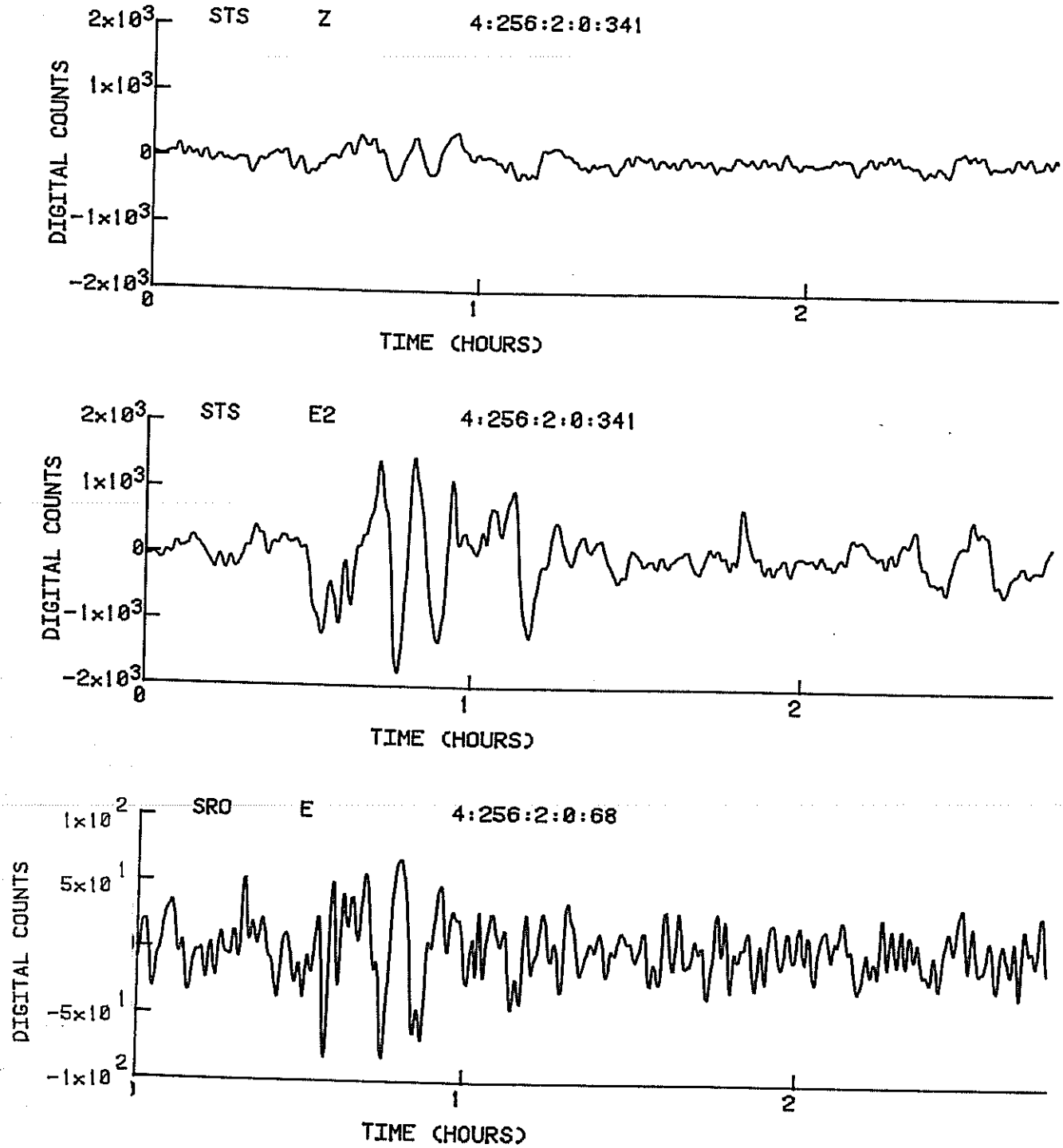

Figure 37.--Waveforms showing examples of signals believed to be caused by infrasonic pressure disturbances. In this reproduction the magnification of the SRO and STS systems is approximately equal at a period of 400 seconds.

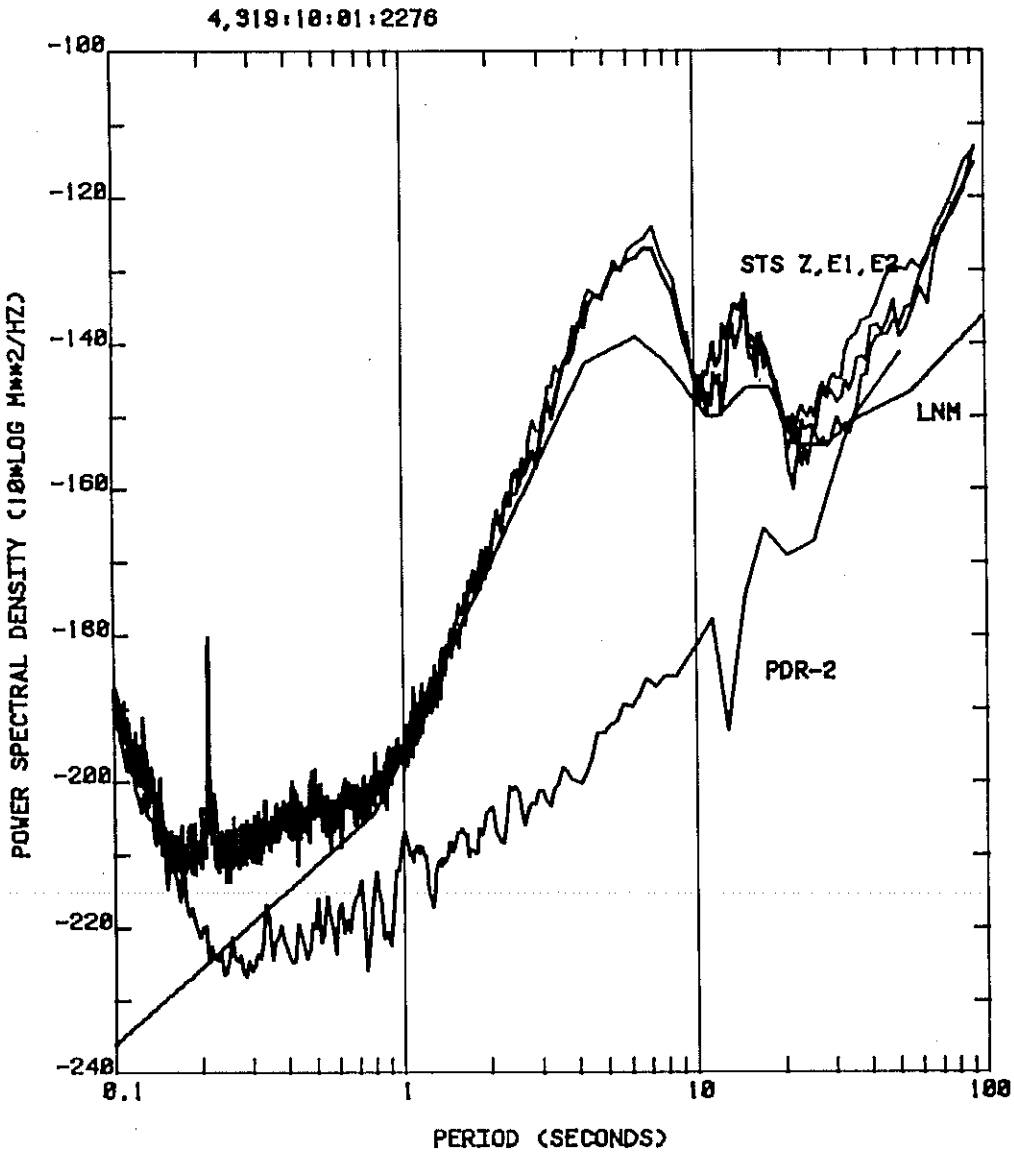

Figure 38.--Power spectral densities computed from signals taken from the three STS-1 BB outputs during a quiet period compared with the LNM curve. The curve labeled PDR-2 is least-count noise of one channel (the other two channels produce the same approximate level of noise power).

4. REFERENCES

Agnew, D.C. and J. Berger, 1978. Vertical seismic noise at very low frequencies, *J. Geophys. Res.*, 83, 5420-5424.

Bowman, H.S. and A.J. Bedard, 1971. Observations of infrasound and subsonic disturbances related to severe weather, *Geophys. J. R. astr. Soc.* 26, 215-242.

Li, T.M.C., J.F. Ferguson, E. Herrin, and H.B. Durham, 1984. High-frequency seismic noise at Lajitas, Texas, *Bull. Seism. Soc. Am.*, 74, 2015-2033.

Murdock, J.N. and C.R. Hutt, 1983. A new event detector designed for the seismic research observatories, *U.S. Geological Survey Open-File Report* 83-785, 37 p.

Peterson, J., 1980. Preliminary observations of noise spectra at the SRO and ASRO stations, *U.S. Geological Survey Open-File Report* 80-992, 25 p.

Sorrells, G.G., 1971. A preliminary investigation into the relationship between long-period seismic noise and local fluctuations in the atmospheric pressure field, *Geophys. J.* 26, 83-98.

Wielandt, E. and G. Streckeisen, 1982. The leaf-spring seismometer: design and performance, *Bull. Seism. Soc. Am.*, 72, 2349-2367.